Article

Immunity

Chronic calcium signaling in IgE$^+$ B cells limits plasma cell differentiation and survival

Graphical abstract

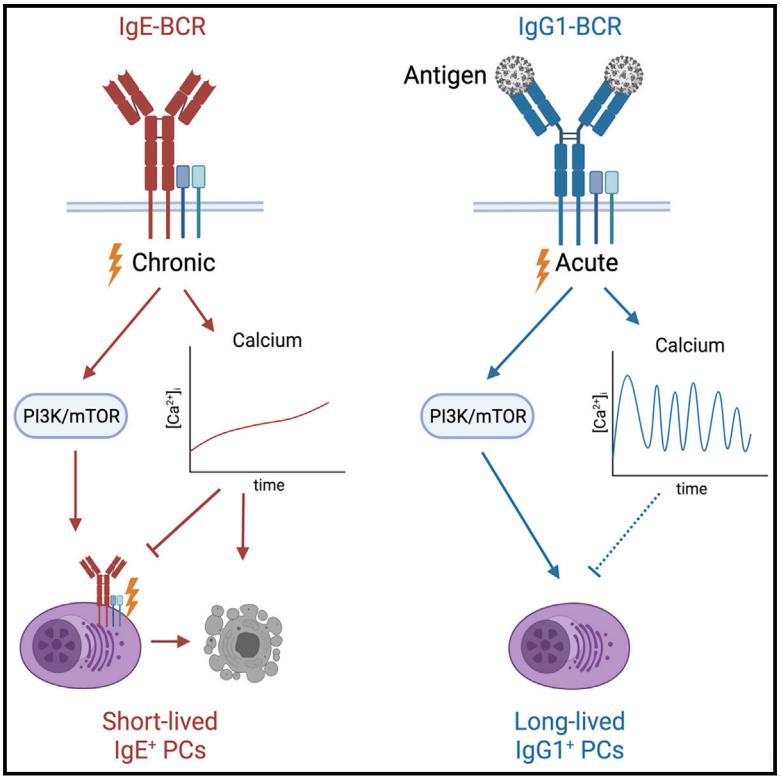

Authors

Rebecca Newman, Pavel Tolar

Correspondence

p.tolar@ucl.ac.uk

In brief

IgE responses are typically transient and do not give rise to long-lived plasma cells (PCs) or memory B cells. Newman and Tolar develop genome-wide CRISPR screens to provide insight into the self-limiting character of IgE responses and find that chronic IgE-BCR signaling sustains intracellular calcium, limiting PC differentiation and triggering BCL2L11-dependent apoptosis.

Highlights

- CRISPR screens identify pathways regulating IgE$^+$ PC differentiation and survival
- PI3K-mTOR signaling promotes IgE$^+$ PC differentiation through IRF4
- Loss of calcium signaling components promotes IgE$^+$ PC differentiation
- Chronic calcium signaling in IgE$^+$ B cells and PCs culminates in apoptosis

Newman & Tolar, 2021, Immunity *54*, 2756–2771
December 14, 2021
https://doi.org/10.1016/j.immuni.2021.11.006

CellPress

CellPress
OPEN ACCESS

Immunity

Article

Chronic calcium signaling in IgE$^+$ B cells limits plasma cell differentiation and survival

Rebecca Newman[1] and Pavel Tolar[1,2,3,*]
[1]Immune Receptor Activation Laboratory, The Francis Crick Institute, 1 Midland Road, London NW1 1AT, UK
[2]Division of Infection and Immunity, Institute of Immunity and Transplantation, University College London, London NW3 2PF, UK
[3]Lead contact
*Correspondence: p.tolar@ucl.ac.uk
https://doi.org/10.1016/j.immuni.2021.11.006

SUMMARY

In contrast to other antibody isotypes, B cells switched to IgE respond transiently and do not give rise to long-lived plasma cells (PCs) or memory B cells. To better understand IgE-BCR-mediated control of IgE responses, we developed whole-genome CRISPR screening that enabled comparison of IgE$^+$ and IgG1$^+$ B cell requirements for proliferation, survival, and differentiation into PCs. IgE$^+$ PCs exhibited dependency on the PI3K-mTOR axis that increased protein amounts of the transcription factor IRF4. In contrast, loss of components of the calcium-calcineurin-NFAT pathway promoted IgE$^+$ PC differentiation. Mice bearing a B cell-specific deletion of calcineurin B1 exhibited increased production of IgE$^+$ PCs. Mechanistically, sustained elevation of intracellular calcium in IgE$^+$ PCs downstream of the IgE-BCR promoted BCL2L11-dependent apoptosis. Thus, chronic calcium signaling downstream of the IgE-BCR controls the self-limiting character of IgE responses and may be relevant to the accumulation of IgE-producing cells in allergic disease.

INTRODUCTION

B cells play crucial roles in immunity by recognizing foreign antigens and eliciting protective responses. Immunoglobulin (Ig) class switching to IgG, IgE, and IgA is a major mechanism to diversify responses and match antibody effector functions to the immune challenge. IgE antibodies, the least abundant antibody class, provide immunity to helminths (Fitzsimmons et al., 2014) and also protect from venoms (Marichal et al., 2013; Starkl et al., 2016) and cancers (Crawford et al., 2018). However, in humans, IgE is also frequently produced in response to innocuous environmental substances such as pollen, dust, or foods, underlying a spectrum of allergic diseases, including life-threatening anaphylaxis (Pawankar, 2014). As such, IgE production needs to be tightly regulated (Laffleur et al., 2015).

IgE responses are initiated by the collaboration of B cells with cognate Th2 cells, which promote class switching to IgE via the cytokine interleukin-4 (IL-4). However, secretion of soluble IgE antibodies first requires expression and signaling of membrane IgE as part of the B cell receptor (BCR) complex (Achatz et al., 1997; Schmitt et al., 2020). The IgE-BCR differs from IgM- and IgG1-BCRs in that it initiates signaling in the absence of antigen, limiting B cell proliferation and stimulating precocious differentiation into IgE$^+$ plasma cells (PCs) (Haniuda et al., 2016; Yang et al., 2012). This mirrors the low and transient IgE$^+$ B cell numbers, their differentiation into short-lived PCs, and the lack of IgE memory B cells *in vivo* (Erazo et al., 2007; He et al., 2013; Yang et al., 2012), arguing that signaling from the IgE-BCR critically regulates IgE production.

Despite the importance of IgE-BCR signaling, the precise mechanisms regulating cellular outcomes remain to be fully understood. Although all membrane-bound Igs associate with the signal-transducing proteins CD79A and CD79B, membrane IgG and IgE also possess a cytoplasmic immunoglobulin tail tyrosine (ITT) motif. The ITT is phosphorylated upon antigen engagement and enhances calcium and MAP kinase (MAPK) signaling through the adaptor GRB2 (Engels et al., 2009). The IgE-BCR also contains a unique extracellular region, which initiates antigen-independent signaling through the membrane adaptor CD19 and through the cytoplasmic adaptor BLNK (Haniuda et al., 2016; Yang et al., 2016). All of these signaling pathways, however, are shared by antigen-stimulated IgG1$^+$ cells, making it unclear how discrete fates of IgE$^+$ B cells are encoded. Proteins specifically binding to either the IgG1- (Liu et al., 2012) or IgE-BCR (Oberndorfer et al., 2006) have been described, but their contributions to this conundrum remain unclear. Additional transcriptional differences between IgG1$^+$ and IgE$^+$ cells and PCs have been noted (Croote et al., 2018; Ramadani et al., 2019), but neither their function nor the role of the paradoxically enhanced surface IgE-BCR expression on IgE$^+$ PCs is known, which contrasts with the well-established decreased expression of IgG1-BCR on IgG1$^+$ PCs (He et al., 2013; Ramadani et al., 2017).

To better understand the mechanisms by which the IgE-BCR controls IgE responses, we employed whole-genome CRISPR

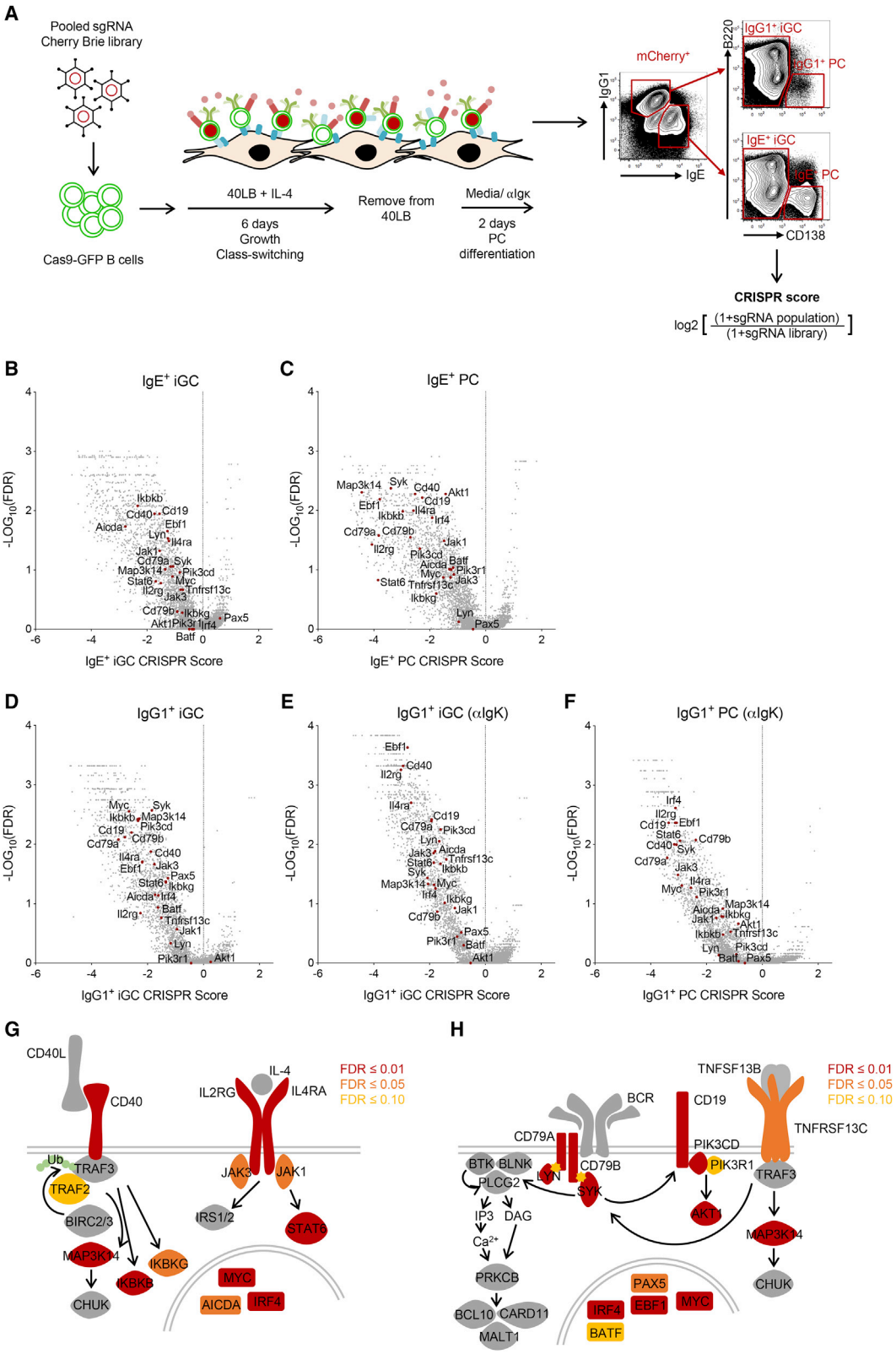

(legend on next page)

screening and identified genes regulating the generation, proliferation, survival, and PC differentiation of IgE^+ and $IgG1^+$ B cells. These experiments confirmed the essential role of antigen-independent IgE-BCR signaling in IgE^+ B cell biology. By comparing IgE^+ cells with $IgG1^+$ cells, we identified common and IgE-specific pathways regulating cell death and PC differentiation. IgE^+ PC differentiation was driven by class-common, but mechanistically distinct, phosphatidylinositide 3-kinase (PI3K)-mammalian target of rapamycin (mTOR) signaling regulating protein levels of the transcription factor IRF4. By contrast, IgE responses were selectively inhibited by calcium signaling, which decreased PC differentiation and persisted in IgE^+ PCs to culminate in their apoptosis. Targeting calcineurin B1 in B cells enhanced IgE^+ PC numbers *in vivo*. Understanding IgE-selective pathways may provide an insight into the accumulation of IgE-producing cells in allergic diseases and offer new targets for treatments.

RESULTS

Genome-wide CRISPR screens in primary B lymphocytes

To evaluate the efficiency of CRISPR-mediated gene editing in primary B cells, we transduced B cells expressing Cas9-GFP (Platt et al., 2014) with mCherry-expressing constructs containing single guide RNAs (sgRNAs) targeting the surface receptor CD22. We cultured the cells in the presence of IL-4 on 40LB feeder cells (Nojima et al., 2011), which express CD40-ligand (CD40L) and tumor necrosis factor ligand superfamily member 13B (TNFSF13B), also known as B cell activating factor (BAFF). By day 8 of the culture, we detected a proportion of insertions or deletions (indels) similar to the proportion of $mCherry^+$ cells, indicating that most transduced cells were edited (Figure S1A). For either of the sgRNAs, this corresponded to more than 80% loss of surface CD22 protein expression (Figure S1B). To test targeting efficiency *in vivo*, we generated chimeras by adoptive transfer of GFP-Cas9-expressing hematopoietic stem cells (HSCs), which were lentivirally transduced with *Cd22* targeting sgRNAs, into lethally irradiated B6.SJL.CD45.1 congenic mice (Figure S1C). Measurement of CD22 levels on peripheral B cells again showed a reduction of CD22 by 67% and 93%, respectively, for the two sgRNAs (Figure S1D).

To identify genes regulating the responses of IgE^+ B cells on a genome-wide scale, we performed pooled CRISPR screens using the Brie library (Doench et al., 2016). To enable screening with this library without drug selection, we cloned the library into a lentiviral plasmid containing mCherry in place of a puromycin selection cassette (Figure S1E). Library complexity was well maintained (Figures S1F and S1G). We infected Cas9-expressing mouse B cells with the Cherry-Brie library and cultured the transduced B cells in the presence of IL-4 on 40LB feeder cells. Naive B cells subjected to this culture rapidly proliferate and express markers characteristic of germinal center (GC) B cells, referred to here as induced GC (iGC) cells, and undergo class switching to IgG1 and IgE (Haniuda et al., 2016; Nojima et al., 2011). After 6 days in culture, we removed B cells from the feeders and cultured them without cytokines for two further days to promote PC differentiation (Figure 1A). Reflecting published data (Kräutler et al., 2017; Phan et al., 2006), IgE^+ cells gave rise to IgE^+ PCs, but $IgG1^+$ PCs were rare without antigen. Stimulation of B cells after feeder removal using anti-Igκ $F(ab')_2$ as a surrogate antigen had no impact on IgE^+ PC differentiation (Figures S1H and S1I) but promoted $IgG1^+$ PC differentiation in a dose-dependent manner (Figures S1J and S1K). We could recapitulate these findings using cultured SW_{HEL} B cells expressing BCRs with hen egg lysozyme (HEL) specificity (Phan et al., 2003) and soluble HEL antigen (data not shown). We therefore included anti-Igκ $F(ab')_2$ in cultures used to screen $IgG1^+$ PCs. At the end of the culture, we flow sorted GFP^+, $mCherry^+$ IgE^+ iGCs, $IgG1^+$ iGCs, IgE^+ PCs, and/or $IgG1^+$ PCs, and amplified and sequenced sgRNAs from each population as well as from the 293T cells used to produce the lentiviral library (Figure 1A). Library complexity was maintained across all screens based on read count distribution for each sgRNA (Figures S2A–S2E). Using the CRISPR screen software MAGeCK (Li et al., 2014) to compare the abundance of sgRNAs in each sorted population with their abundance in the original sgRNA library, we identified sgRNAs that were enriched or depleted in our populations of interest and assigned positive or negative CRISPR scores, respectively, to genes inhibiting or promoting each population (Figure 1A; Table S1). To verify that our screening was successful, we compared the CRISPR scores of 187 common essential genes (Wang et al., 2015) and nontargeting sgRNAs with all genes in the library. CRISPR scores across the library showed a range of values, whereas CRISPR scores of essential genes were negative and CRISPR scores of nontargeting controls remained close to zero (Figures S2F–S2O).

RNA sequencing (RNA-seq) data confirmed that the populations generated in the *in vitro* culture were transcriptionally distinct (Figure S3A) and expressed key transcripts associated with GC (*Bcl6*, *Pax5*) or PC (*Prdm1, Irf4, Xbp1*) fates (Figures S3B–S3F; Table S2), as well as the correct Igh genes (Figures S3G–S3I). Furthermore, CRISPR scores of genes known to encode signaling components downstream of the BCR, CD40, BAFF receptor (BAFF-R), and IL-4 receptor (IL-4R) were negative across all cell populations (Figures 1B–1H and S3J–S3M).

To demonstrate that the screens identified genes not previously shown to be important in B cells, we validated the essentiality of *Morc3* (Figures S4A and S4B), a gene silencer binding to H3K4me3 marked chromatin (Li et al., 2016), which is phosphorylated after BCR stimulation (Satpathy et al., 2015). To test the role of *Morc3 in vivo*, we generated chimeras by adoptive transfer of GFP-Cas9-expressing HSCs, which were lentivirally

Figure 1. Genome-wide CRISPR screens in primary B lymphocytes

(A) Schematic of screen workflow and sorting strategy.

(B–F) Volcano plots showing gene CRISPR scores versus statistical significance corrected for false discovery rate (FDR) for all genes (gray) and selected B cell-essential genes (dark red). The plots show CRISPR screens of IgE^+ iGCs (B), IgE^+ PCs (C), $IgG1^+$ iGCs (D), and $IgG1^+$ iGCs cultured with anti-Igκ $F(ab')_2$ (E), and $IgG1^+$ PCs cultured with anti-Igκ $F(ab')_2$ (F).

(G and H) Schematics showing CD40 and IL-4 signaling (G), BCR and BAFF-R signaling (H), indicating minimum FDR ($\leq$0.01 dark red, $\leq$0.05 orange, $\leq$0.10 yellow, >0.1 gray) across all screens for indicated gene products. PLCG2 was not targeted by the library.

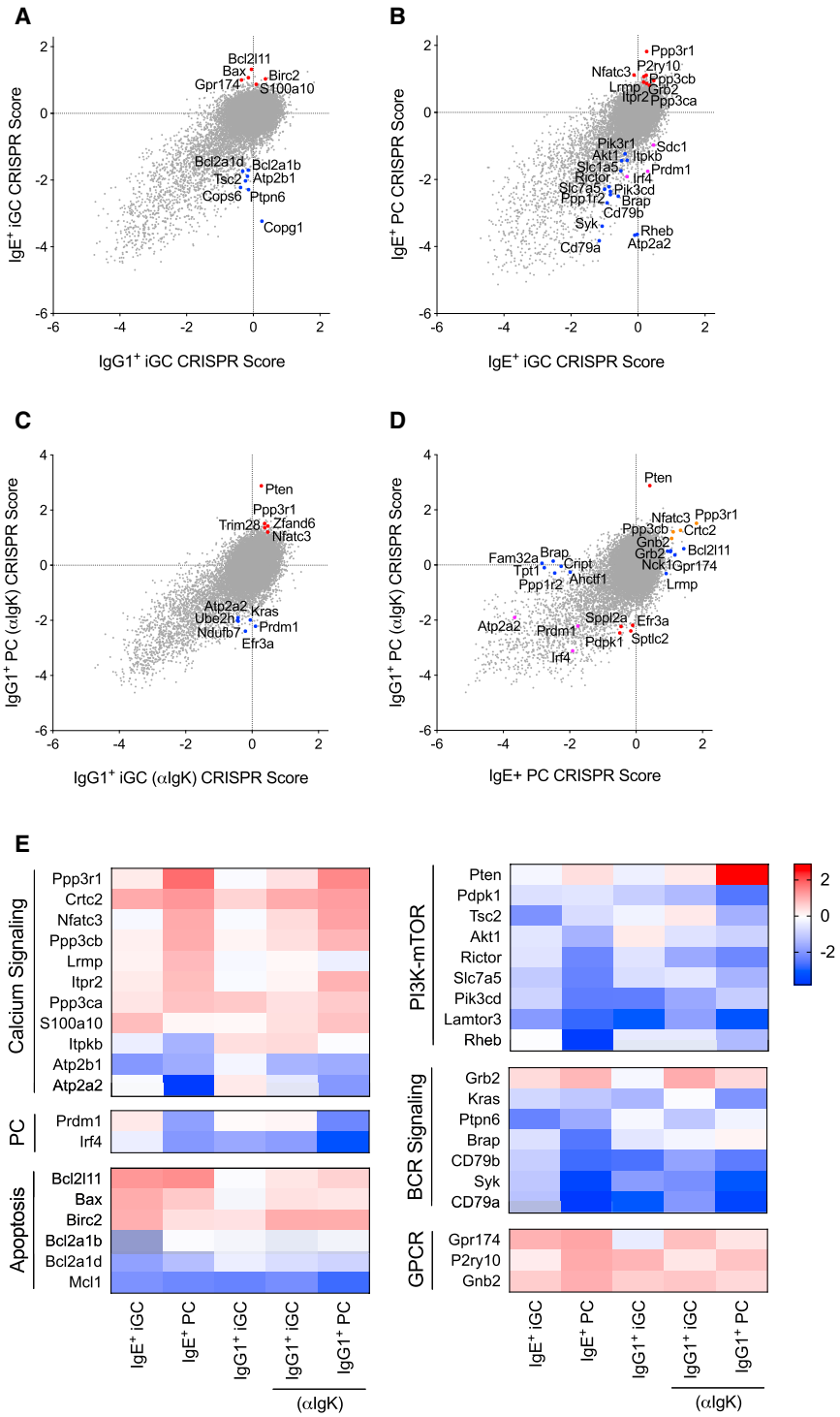

Figure 2. Comparison of CRISPR scores from IgE$^+$ and IgG1$^+$ screens identifies unique regulators of IgE$^+$ B cell survival, proliferation, and differentiation

(A) Dot plot comparing CRISPR scores from the IgE$^+$ and IgG1$^+$ iGC screens. Key IgE$^+$ iGC specific essential genes (blue points) and negative regulators (red points) are indicated.

(B) Dot plot comparing CRISPR scores from IgE$^+$ PC and iGC screens. Key IgE$^+$ PC-specific essential genes (blue points) and negative regulators (red points) are indicated. Known PC regulators are shown in pink.

(C) Dot plot comparing CRISPR scores from IgG1$^+$ PC and iGC screens performed with anti-Igκ F(ab′)$_2$. Key IgG1$^+$ PC-specific essential genes (blue points) and negative regulators (red points) are indicated.

(D) Dot plot comparing CRISPR scores from IgE$^+$ PC and IgG1$^+$ PC with anti-Igκ F(ab′)$_2$ screens. Key IgG1$^+$ PC-specific genes (blue points) and IgE$^+$ PC-specific genes (red points) are shown, with PC common essential genes (pink points) and negative regulators (orange points) indicated.

(E) Heat maps showing CRISPR scores across all five screens of genes from filtered gene lists (Tables S3–S6). Genes are grouped based on functional enrichments identified using STRING analysis (Szklarczyk et al., 2019).

transduced with *Morc3* targeting sgRNA, into sublethally irradiated recombination activating gene 1 (RAG1$^{-/-}$) mice. In these chimeras, we identified *Morc3*-targeted cells using mCherry expression and found a substantial reduction in the proportion of mature splenic B cells compared with a *Cd4*-targeting control or to nontargeted mCherry$^-$ cells (Figures S4C–S4G). Targeting *Morc3* had no effect on the proportion of CD4 T cells (Figure S4H); thus, *Morc3* has a critical role specifically in B cell development.

Comparison of CRISPR scores from IgE$^+$ and IgG1$^+$ screens identifies unique regulators of IgE$^+$ B cell survival, proliferation, and differentiation

To identify genes regulating IgE$^+$ cells selectively, we compared CRISPR scores between populations (Figures 2A–2D). By selecting for genes that had a significantly negative CRISPR score in the IgE$^+$ iGC screen but not in the IgG1$^+$ iGC screen, we identified genes that were essential only in IgE$^+$ iGC cells (Figure 2A; Table S3). Similarly, by selecting genes with a significantly positive IgE$^+$ iGC CRISPR score but with IgG1$^+$ iGC CRISPR scores near zero, we identified genes that selectively inhibited IgE$^+$ iGC cells (Figure 2A; Table S3). We removed genes that were not expressed according to RNA-seq (Figure S3; Tables S2 and S3). Pathways enriched in each gene list were identified using STRING (Szklarczyk et al., 2019) (Figure 2E). This revealed a key role for BCR signaling and apoptosis in regulating IgE iGCs (Figures 2A and 2E). Although apoptosis has been reported to limit IgE$^+$ B cell expansion (Haniuda et al., 2016; Laffleur et al., 2015), its importance remains contentious (Yang et al., 2016) and will be explored further in the next sections.

To identify regulators of IgE$^+$ PC differentiation and survival, we compared CRISPR scores from IgE$^+$ iGCs with those of IgE$^+$ PCs (Figure 2B). We captured *Irf4* and *Prdm1*, the central regulators of PC differentiation, and *Sdc1*, which encodes CD138 used to sort this population (Figure 2B (pink dots); Table S4). We validated that *Irf4* and *Prdm1* were essential for IgE$^+$ PCs (Figures S4I and S4J, respectively) and were efficiently targeted (Figures S4K and S4L). Among the hits from this analysis, which included a number of chromatin and transcriptional regulators, STRING identified two major signaling pathways connected with the BCR: PI3K-mTOR, which was essential for IgE$^+$ PCs, and calcium-calcineurin-NFAT, which was inhibitory (Figures 2B and 2E; Table S4).

To identify which of these regulators were unique for IgE$^+$ PCs, we also compared CRISPR scores from IgG1$^+$ iGCs with those of IgG1$^+$ PCs where anti-Igκ F(ab′)$_2$ was used to support IgG1$^+$ PC differentiation (Figures 2C and S1). This indicates that the calcineurin-NFAT pathway also plays an inhibitory role in IgG1$^+$ PC (Figures 2C–2E; Tables S5 and S6). However, some regulators of calcium signaling were unique to IgE$^+$ PCs, including GRB2 and LRMP (Shindo et al., 2010), as was the pro-apoptotic protein BCL2L11, suggesting that calcium and apoptosis may uniquely regulate IgE$^+$ PCs (Figures 2D and 2E; Table S6).

The PI3K-mTOR pathway promotes IgE$^+$ PC differentiation by enhancing IRF4 protein levels

PI3K signaling, stimulated by the IgE-BCR, has been proposed to promote IgE$^+$ PC differentiation (Haniuda et al., 2016; Yang et al., 2016), but the mechanisms remain unclear. Our data suggest that this pathway regulates PC differentiation through mTOR. Both *Rheb*, a positive regulator of mTOR activity, and *Slc7a5*, an amino acid transporter required for mTOR activation, were essential for IgE$^+$ PC differentiation (Figures 2B, 3A, and 3B). These requirements were shared with IgG1$^+$ PCs induced by anti-Igκ F(ab′)$_2$ (Figures 3A and 3B). However, *Slc7a5* was also essential for IgE$^+$ but not for IgG1$^+$ iGCs (Figure 3B). This may result from differences in proliferation because class switching to IgE requires more rounds of cell division than those required for IgG1 (Hasbold et al., 1998). Although proliferation was decreased in both *Slc7a5*- and *Rheb*-deficient iGC cells, both IgE$^+$ and IgG1$^+$ PC proportions were still decreased when normalized per cell division. *Slc7a5*-deficient IgE$^+$ iGCs were also decreased when normalized per cell division, indicating that the role of mTOR was independent of proliferation (Figures S5A–S5I). *Tsc2*, a negative regulator of *Rheb*, was also essential in IgE$^+$ iGC cells and negatively regulated both IgE$^+$ and IgG1$^+$ PCs (Figures 2A and 3C). Proliferation of *Tsc2*-deficient cells was not different to nontargeted cells (Figures S5J and S5K). To confirm the importance of the mTOR pathway, we cultured B cells with the mTOR inhibitor, rapamycin, and observed a specific loss of IgE$^+$ iGC cells as well as decreased IgE$^+$ and IgG1$^+$ PC differentiation (Figure 3D). Both IgE$^+$ and IgG1$^+$ iGC cells cultured with rapamycin proliferated less than the cells cultured with vehicle control (Figures S5L and S5M). We also saw a specific loss of PCs when cells were cultured with rapamycin after class switching had occurred (Figures S5N–S5P). Thus, regulation of mTOR is selectively essential for IgE$^+$ B cells, whereas mTOR activity promotes both IgE$^+$ and IgG1$^+$ PC differentiation.

The PI3K-mTOR pathway acts upstream of IRF4, a key transcription factor needed to initiate PC differentiation by upregulating PRDM1 (Haniuda et al., 2016; Sciammas et al., 2006); however, the molecular mechanism remains unknown. mTOR activity was elevated in both IgE$^+$ PCs and IgG1$^+$ PCs when compared with IgE$^+$ and IgG1$^+$ iGCs, respectively, using staining for phosphorylated mTOR or its substrate S6 kinase (Figures S5Q and S5R). We found that *Irf4* mRNA was increased in IgE$^+$ and IgG1$^+$ PCs but was not different between IgE$^+$ and IgG1$^+$ iGCs by RNA-seq (Figure S5S) and by RT-PCR (Figure 3E). However, IRF4 protein was elevated in a subset of IgE$^+$ iGCs relative to IgG1$^+$ iGCs, in addition to the up-regulation in IgE$^+$ and IgG1$^+$ PCs (Figure 3F). Rapamycin eliminated the IRF4^{hi} PRDM1^{hi} IgE$^+$ iGC population and decreased IRF4 protein levels in both IgE$^+$ and IgG1$^+$ PCs (Figures 3G and 3H). Although rapamycin decreased *Irf4* transcript in IgG1$^+$ PCs, it did not affect *Irf4* mRNA in IgE$^+$ iGCs or IgE$^+$ PCs (Figure 3E). Thus, although IgE-BCR signaling to mTOR may be too weak to activate *Irf4* transcription, it elevates IRF4 protein in a fraction of IgE$^+$ B cells post-transcriptionally.

Calcium signaling negatively regulates IgE$^+$ PC differentiation

The top-ranked negative regulators of IgE$^+$ PC differentiation were genes involved in BCR calcium signaling (Figures 2B, 2D, and 2E; Tables S4 and S6). This included *Grb2*, which potentiates calcium signaling downstream of class-switched BCRs, the endoplasmic reticulum (ER)-localized calcium channel *Itpr2*, and members of the calcineurin-NFAT pathway (*Ppp3r1*, *Ppp3cb*, *Ppp3ca*, *Nfatc3*). In contrast, *Itpkb*, which negatively regulates calcium signaling by converting IP_3 to IP_4, promoted IgE$^+$ PC differentiation. We also observed essential roles in IgE$^+$ iGCs and PCs for genes controlling calcium homeostasis by removing calcium from the cytosol, such as the SERCA pump *Atp2a2* and the plasma membrane calcium pump *Atp2b1* (Figures 2A and 2B; Tables S3 and S4). We validated the importance of *Grb2* both *in vitro* and *in vivo* (Figures S6A–S6C) and *Itpr2* and the calcineurin-NFAT pathway by testing 2 sgRNAs targeting each gene in individual assays. IP_3R-2 was inhibitory for IgE$^+$ PCs and IgG1$^+$ PCs, whereas IP_3R-3 (encoded by *Itpr3*) had only a small effect in IgG1$^+$ PCs (Figures S6D and S6E), indicating nonredundant roles for IP_3Rs in B cells. *Ppp3r1* (calcineurin subunit B1) and *Nfatc3* targeting resulted in a specific expansion of IgE$^+$ and IgG1$^+$ PCs, with *Ppp3r1* targeting having a stronger effect on IgE$^+$ than on IgG1$^+$ PCs ($p = 0.002$ when comparing the fold-change increase using a paired t test) (Figures 4A and 4B). Targeting *Crtc2*, which is activated following dephosphorylation by calcineurin (Altarejos and Montminy, 2011), also resulted in specific expansion of IgE$^+$ PCs and antigen-stimulated IgG1$^+$ PCs *in vitro*, although this did not reach statistical significance (Figure S6F). By contrast, *Plcg2* was essential for both IgE$^+$ and IgG1$^+$ PCs, illustrating that the inhibitory effect of this pathway is selective to the mechanisms downstream of IP_3 (Figure S6G).

The effect of the calcineurin-NFAT pathway was primarily through PC differentiation rather than cell death or proliferation, as illustrated by unchanged proportions of annexin V$^+$ PCs between either *Ppp3r1*- or *Nfatc3*-sufficient and -deficient cells (Figures 4C and 4D) and similar cell division (Figures 4E and 4F).

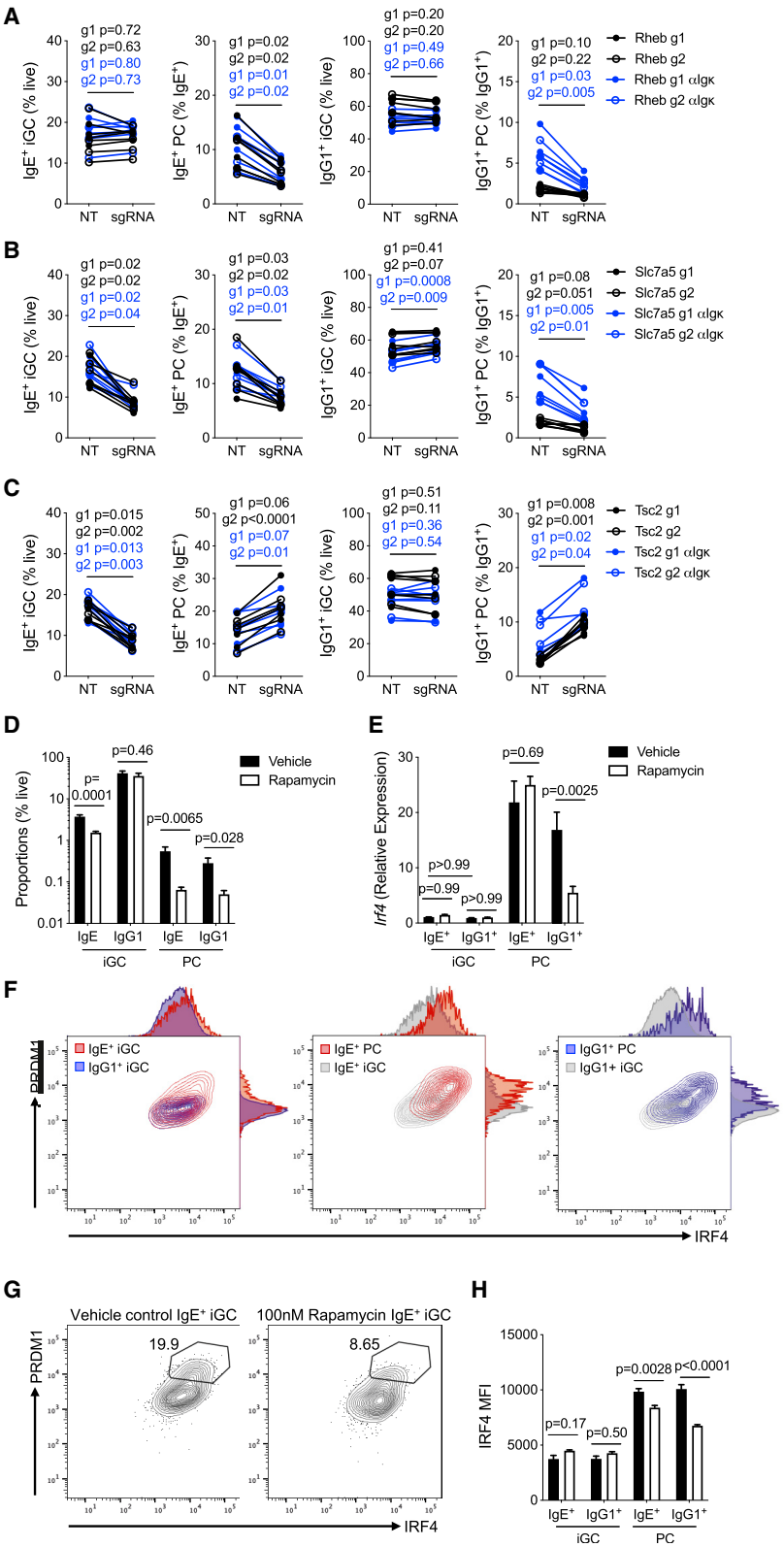

Figure 3. mTOR signaling drives IgE$^+$ PC differentiation through post-transcriptional regulation of IRF4

(A) Targeting of *Rheb* in iGC cultures using 2 sgRNAs not present in the Cherry-Brie library. sgRNA 1 and 2 (g1 and g2) shown as open and closed circles, each point represents a replicate. Conditions where 500 ng/ml anti-Igκ F(ab′)$_2$ was added for the final 2 days of culture shown in blue. Proportions of IgE$^+$ iGCs, IgE$^+$ PCs, IgG1$^+$ iGCs, and IgG1$^+$ PCs (graphs from left to right) shown for non-targeted (NT) (GFP$^+$ mCherry$^-$) and targeted (sgRNA) (GFP$^+$ mCherry$^+$) comparing cells within the same well (connected by a line).

(B) Targeting of *Slc7a5*, as described for (A).

(C) Targeting of *Tsc2*, as described for (A). Data in (A–C) were pooled from four separate experiments.

(D) Proportions of iGCs and PCs (as % of live lymphocytes) in iGC cultures where 100 nM rapamycin (white bars) or vehicle control (black bars) was added for the final 5 days of culture. n = 8 biological replicates pooled from four independent experiments.

(E) *Irf4* transcript abundance relative to *Hprt* and *Tbp* in sorted IgE$^+$ and IgG1$^+$ iGCs and PCs. n = 3 biological replicates. Cells were cultured as described for (D).

(F) Representative flow plots indicating PRDM1 versus IRF4 protein expression in IgE$^+$ iGCs (red), overlaid with IgG1$^+$ iGCs (blue) (left), IgE$^+$ iGCs (gray), overlaid with IgE$^+$ PCs (red) (middle), and IgG1$^+$ iGCs (gray) overlaid with IgG1$^+$ PC (blue) (right), with adjunct histograms. Data are representative of 14 technical replicates from three independent experiments.

(G) Representative plots indicating PRDM1 versus IRF4 protein expression in IgE$^+$ iGCs. Cells were cultured as described for (D). Gates indicate proportions of cells in the IRF4^{hi} PRDM1^{hi} population. n = 3 biological replicates pooled from two independent experiments.

(H) MFI of IRF4 in flow cytometry in IgE$^+$ and IgG1$^+$ iGCs and PCs. Cells were cultured as described for (D). n = 3 biological replicates.

p values indicated using paired t test (A–C), unpaired t test (D), or two-way ANOVA with Sidak's multiple comparisons test (E and H). Bars indicate mean ± SEM.

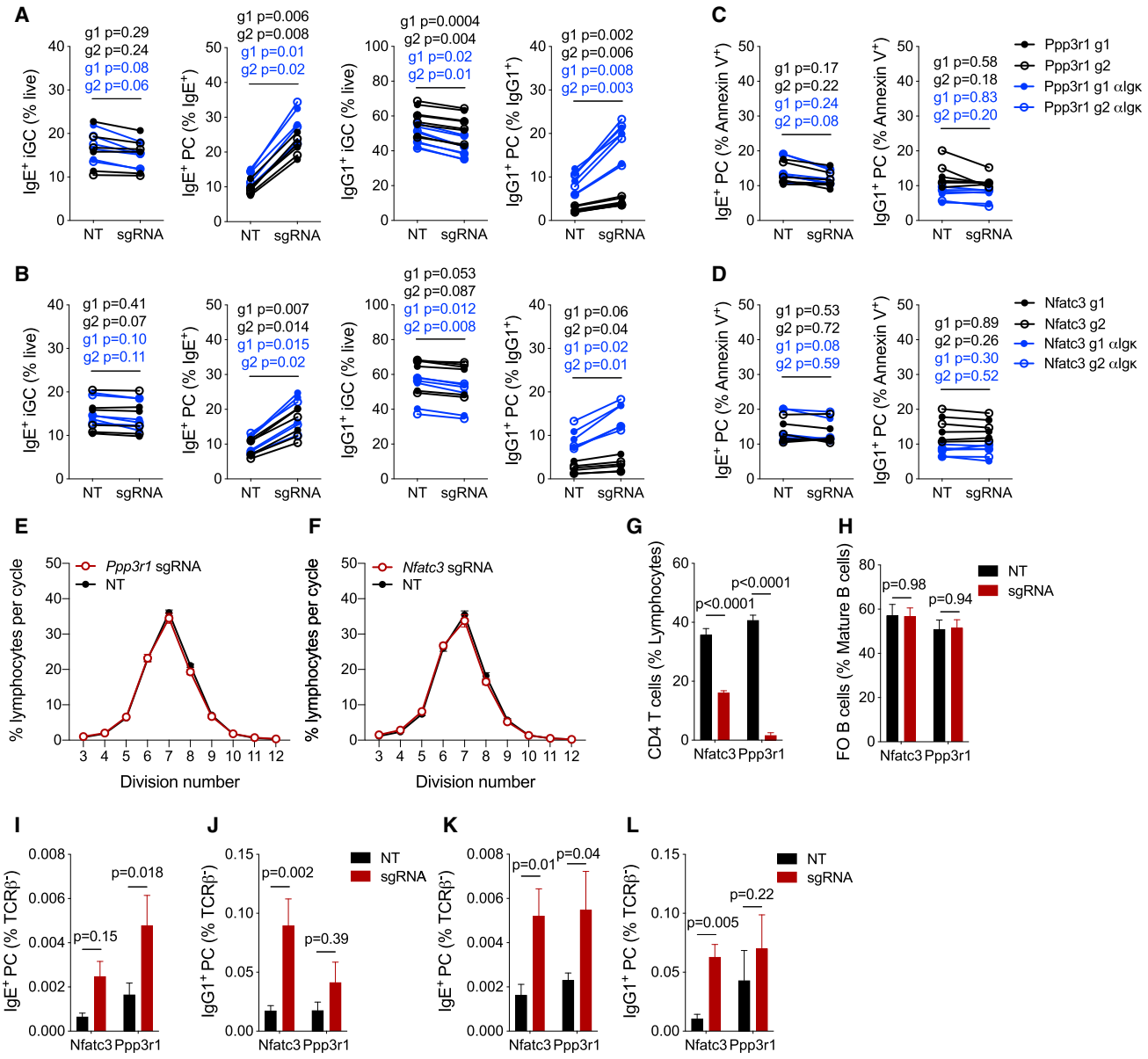

Figure 4. Calcium signaling negatively regulates IgE$^+$ PC differentiation

(A) Targeting of *Ppp3r1* in iGC cultures using 2 sgRNAs not present in Cherry-Brie library. sgRNA 1 and 2 (g1 and g2) shown as open and closed circles, each point represents a replicate. Conditions where 500 ng/ml anti-Igκ F(ab′)$_2$ was added for the final 2 days of culture shown in blue. Proportions of IgE$^+$ iGCs, IgE$^+$ PCs, IgG1$^+$ iGCs, and IgG1$^+$ PCs (graphs from left to right) shown for nontargeted (NT) (GFP$^+$ mCherry$^-$) and targeted (sgRNA) (GFP$^+$ mCherry$^+$) comparing cells within the same well (connected by a line).

(B) Targeting of *Nfatc3*, as described for (A).

(C and D) Proportions of annexin V$^+$ IgE$^+$ PCs, and IgG1$^+$ PCs shown for nontargeted (NT) and *Ppp3r1*-targeted (C) or *Nfatc3*-targeted (D) (sgRNA) cells, as described for (A). Data in (A–D) were pooled from three separate experiments.

(E and F) Proportions of total lymphocytes in each division cycle comparing *Ppp3r1*-targeted cells (red line) to nontargeted cells (black line) (E), *Nfatc3*-targeted cells (red line) to nontargeted cells (black line) (F).

(G–J) Proportions of splenic CD4 T cells (G), splenic follicular B cells (H), dLN IgE$^+$ PCs (I), and dLN IgG1$^+$ PCs (J) at day 7 post-immunization with NP-CGG in alum in CRISPR-Cas9 chimeras. n = 8 biological replicates pooled from two independent experiments.

(K and L) Proportions of dLN IgE$^+$ PCs (K) and dLN IgE$^+$ PCs (L) at day 7 in NP-CGG in alum-immunized chimeras in which Cas9 expression is restricted to the B cell lineage. n = 8–10 biological replicates pooled from two independent experiments.

In (G–L), nontargeted (NT) GFP$^+$ mCherry$^-$ cells are shown as black bars and targeted (sgRNA) GFP$^+$ mCherry$^+$ cells are shown as red bars. p values indicated using paired t test (A–D) and two-way RM ANOVA with Sidak's multiple comparisons test (G–L). Bars indicate mean ± SEM.

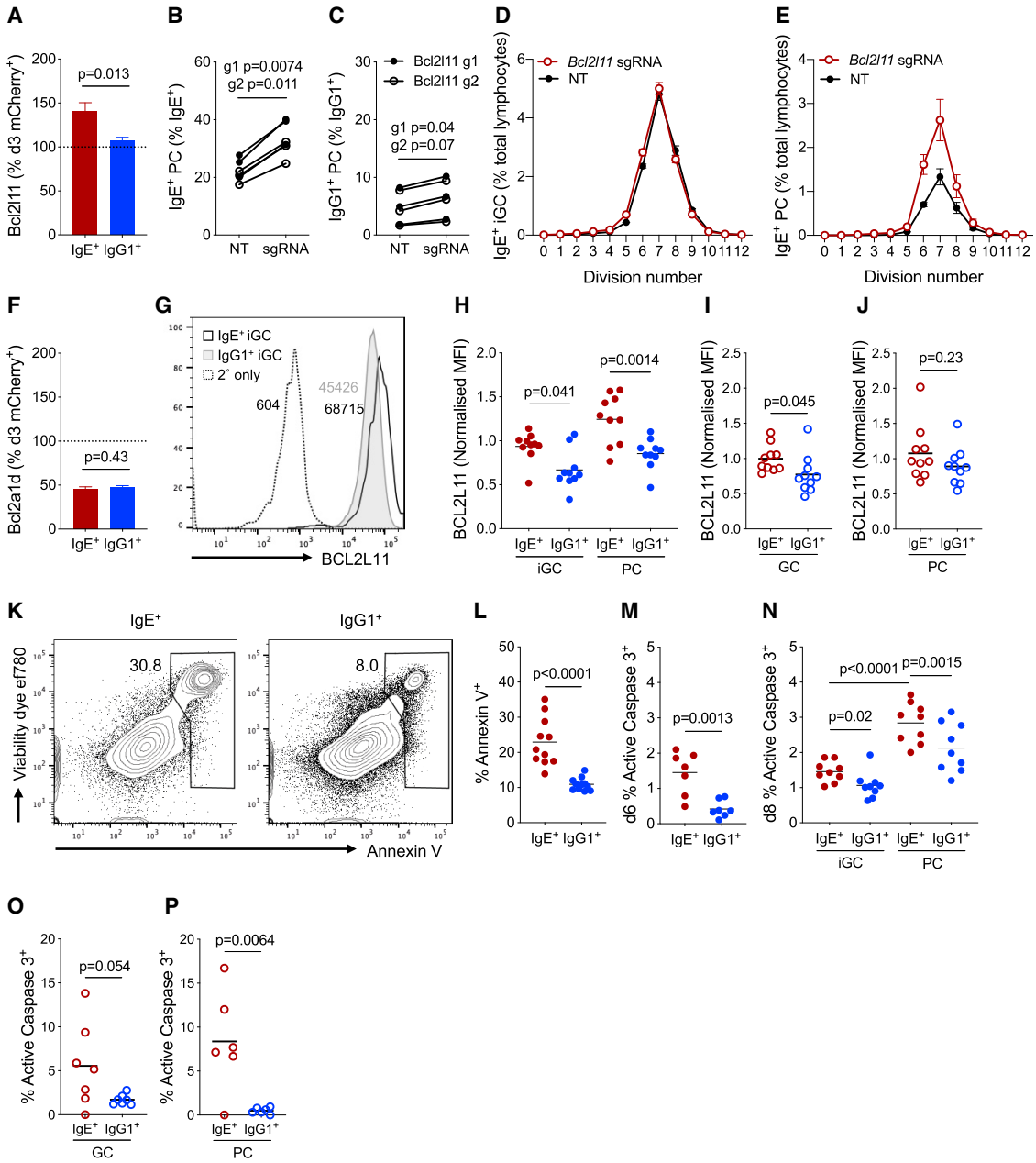

Figure 5. IgE$^+$ B cells and PCs undergo increased apoptosis mediated by BCL2L11

(A) Normalized IgE$^+$ and IgG1$^+$ cell numbers following *Bcl2l11*-targeting shown as proportions of mCherry$^+$ cells at day 8 of the culture relative to mCherry$^+$ cells at day 3. Data pooled from effects of 2 sgRNAs per gene, in two independent experiments.

(B and C) Targeting of *Bcl2l11* in iGC cultures using 2 sgRNAs not present in Cherry-Brie library. sgRNA 1 and 2 (g1 and g2) shown as open and closed circles, each point represents a replicate. Proportions of IgE$^+$ PCs (B) and IgG1$^+$ PCs (C) shown for nontargeted (NT) (GFP$^+$ mCherry$^-$) and targeted (sgRNA) (GFP$^+$ mCherry$^+$) comparing cells within the same well (connected by a line). Data are pooled from two independent experiments.

(D and E) Proportions of IgE$^+$ iGCs (D) and IgE$^+$ PCs (E) in each division cycle comparing *Bcl2l11*-targeted cells (red line) to nontargeted cells (black line).

(F) IgE$^+$ and IgG1$^+$ cell numbers following *Bcl2a1d*-targeting, as described for (A).

(G) Representative flow plot showing BCL2L11 expression in IgE$^+$ iGCs (black line) and IgG1$^+$ iGCs (gray filled histogram) from day 8 of iGC culture. Secondary antibody staining shown as a dashed line. Median fluorescence intensity (MFI) for each histogram is indicated.

(H) Normalized MFI for BCL2L11 staining from day 8 of *in vitro* culture. Data are pooled from three independent experiments.

(I and J) Normalized MFI for BCL2L11 staining in GC B cells (I) and PCs (J) at day 7 post-immunization with NP-CGG in alum. Data are pooled from two independent experiments.

(K) Representative flow plots showing proportion of annexin V$^+$ IgE$^+$ and IgG1$^+$ cells (including iGCs and PCs) from day 8 of iGC cultures.

(L) Proportion of annexin V$^+$ cells as described in (K).

(M) Proportion of active caspase-3$^+$ cells from day 6 of iGC culture. Data are pooled from two experiments.

(legend continued on next page)

To validate our findings in *in vivo*, we generated lentiviral chimeras, as described for *Morc3*. Upon the deletion of *Nfatc3* and *Ppp3r1*, we observed a loss of CD4 T cells (Canté-Barrett et al., 2007; Neilson et al., 2004), but proportions of mature B cells were unchanged (Figures 4G and 4H). At day 7 post-immunization, we observed an increased proportion of GC B cells in the draining LNs (dLNs) in both the *Nfatc3*- and *Ppp3r1*-deficient compartments (Figures S6H–S6J). There was an increase in the overall proportion of PCs in *Nfatc3*-deficient cells (Figure S6K) with a stronger effect in IgG1$^+$ PCs (Figures 4I and 4J). By contrast, *Ppp3r1* targeting resulted in a selective increase of IgE$^+$ PCs (Figure 4I). These findings were reproduced in chimeras in which Cas9 expression was restricted to B cells, indicating that they were cell intrinsic (Figures 4K, 4L, and S6L–S6O). Thus, signaling through calcineurin NFATC3 restricts IgE$^+$ and IgG1$^+$ PC numbers *in vitro* and *in vivo*, and calcineurin B1 is a stronger inhibitor of IgE$^+$ cells than IgG1$^+$ cells.

IgE$^+$ B cells and PCs undergo increased apoptosis mediated by BCL2L11

Our screen data suggested that the survival of IgE$^+$ iGCs and PCs is regulated by specific BCL2 family proteins, namely, pro-apoptotic BCL2L11 (BIM) and BAX and anti-apoptotic BCL2A1B and D (Figures 2 and S3K; Table S3). Deletion of *Bcl2l11* resulted in preferential expansion of IgE$^+$ cells (Figure 5A) and IgE$^+$ PCs (Figure 5B), with a smaller impact on IgG1$^+$ PCs (Figure 5C). This was not due to increased proliferation (Figures 5D and 5E). Targeting *Bcl2a1d* resulted in loss of both IgE$^+$ and IgG1$^+$ cells (Figure 5F). Levels of BCL2L11 protein were higher in IgE$^+$ iGCs than in IgG1$^+$ iGCs and even higher in IgE$^+$ PCs (Figures 5G and 5H). We also found increased BCL2L11 expression in IgE$^+$ GC B cells compared with IgG1$^+$ GC B cells in mice immunized with NP-CGG in alum and a similar trend in PCs (Figures 5I and 5J). Further supporting the role of apoptosis in limiting IgE$^+$ B cells, we observed increased proportions of annexin V$^+$ and active caspase-3$^+$ IgE$^+$ cells in the culture relative to IgG1$^+$ cells (Figures 5K–5N). The proportion of active caspase-3$^+$ cells was also higher in IgE$^+$ PCs than in IgG1$^+$ PCs from immunized mice, with a similar trend observed for GC B cells (Figures 5O and 5P). Together, these data suggest that compared with IgG1$^+$ cells, IgE$^+$ cells undergo increased apoptosis both *in vitro* and *in vivo* and that this apoptosis involves BCL2L11 and culminates in PCs.

Calcium signaling downstream of the IgE-BCR drives apoptosis in IgE$^+$ B cells and PCs

To understand what triggers apoptosis in IgE$^+$ cells, we investigated the pro-apoptotic role of BCR signaling. We showed that IgE$^+$ iGCs selectively required *Ptpn6* (which encodes for the inhibitory tyrosine phosphatase SHP1) (Figure 6A). Treating cells for the final 48 h of culture with the Syk inhibitor (BAY 61-3606) increased proportions, and decreased cell death of IgE$^+$ iGCs but decreased proportions and increased cell death of IgG1$^+$ iGCs (Figures 6B–6E). Syk inhibition also decreased cytosolic calcium levels in both subsets (Figures 6F and 6G), suggesting that BCR signaling driving calcium release from the ER may be important for apoptosis. Deletion of *Grb2*, a potentiator of calcium signaling, resulted in the expansion of IgE$^+$ iGCs and IgE$^+$ PCs, but loss of *Grb2* was detrimental to antigen-dependent IgG1$^+$ PC differentiation and/or survival (Figure S6A). Consistently, *Grb2*$^{fl/fl}$*Cd79a*$^{cre/+}$ mice had increased proportions of IgE$^+$ GC B cells (Figure S6B) and decreased IgG1$^+$ GC B cells after immunization (Figure S6C) compared with *Grb2*$^{fl/fl}$ littermate controls. PLCG2 promoted apoptosis in IgE$^+$ PCs (Figure S7A), despite being required by both IgE$^+$ and IgG1$^+$ PCs (Figure S6G), as indicated previously (Hikida et al., 2009). Finally, targeting *Itpkb*, a negative regulator of calcium signaling, resulted in a loss of IgE$^+$ iGCs and decreased IgE$^+$ PC proportion, which was associated with enhanced apoptosis in PCs (Figures S7B and S7C). Thus, mechanisms that enhance calcium signaling downstream of the IgE-BCR act to limit IgE$^+$ B cell responses by promoting apoptosis in both IgE$^+$ B cells and PCs.

To understand why IgE$^+$ iGCs and IgE$^+$ PCs were more sensitive to increases in cytosolic calcium, we analyzed calcium flux. We observed that IgE$^+$ iGCs fluxed calcium to the same extent as IgG1$^+$ iGCs in response to thapsigargin, ionomycin, or anti-Igκ F(ab′)$_2$ (data not shown), but baseline calcium levels were greater and increased further in IgE$^+$ PCs (Figures 6H (colored arrows) and 6I). We hypothesized that chronic IgE-BCR signaling may persist after differentiation into PCs because of elevated surface expression of the IgE-BCR on IgE$^+$ PCs compared with iGCs (Figures 6J and 6K) (He et al., 2013; Ramadani et al., 2017). Although treatment with the Syk inhibitor (BAY 61-3606) blocked IgE$^+$ PC differentiation (Figure 6L), culturing sorted IgE$^+$ PCs in the presence of BAY 61-3606 for 20 h resulted in decreased proportions of active caspase-3$^+$ cells compared with vehicle controls (Figure 6M), suggesting that although Syk is required for PC differentiation, it continues to signal in IgE$^+$ PCs and that this is detrimental for their survival.

Time-lapse microscopy showed that IgE$^+$ B cells maintained steady calcium levels, although a higher percentage of IgG1$^+$ B cells underwent calcium oscillations (Figures 6N–6Q) that were further enhanced by the presence of anti-Igκ F(ab′)$_2$ for the final 2 days of the *in vitro* cultures (Figures 6O, 6Q, and 6R). Thus, in contrast to antigen-induced calcium oscillations in IgG1$^+$ cells, IgE$^+$ cells experience a sustained elevation of intracellular calcium levels, which is associated with apoptosis.

Elevated cytosolic calcium in IgE$^+$ B cells drives mitochondrial apoptosis through BCL2L11

To test whether sustained cytosolic calcium alone could trigger apoptosis of IgE$^+$ cells, we tested the roles of the calcium transporters *Atp2b1* and *Atp2a2* identified by the screen. Targeting *Atp2b1* led to elevated baseline intracellular calcium in all cell

(N) Proportion of active caspase-3$^+$ cells from day 8 of iGC culture. Data are pooled from two experiments.
(O and P) Proportion of active caspase-3$^+$ cells in GC B cells (O) and PCs (P) at day 7 post-immunization with NP-CGG in alum. Data are pooled from two independent experiments.
p values indicated using unpaired t test (A, F, I, J, L, M, O, and P), paired t test (B, C, and N) one-way ANOVA with Tukey's multiple comparisons test (H). Bars indicate mean ± SEM. In (H and L–N) each dot represents a technical replicate, line indicates mean. In (I, J, O, and P) each dot represents a biological replicate, line indicates mean.

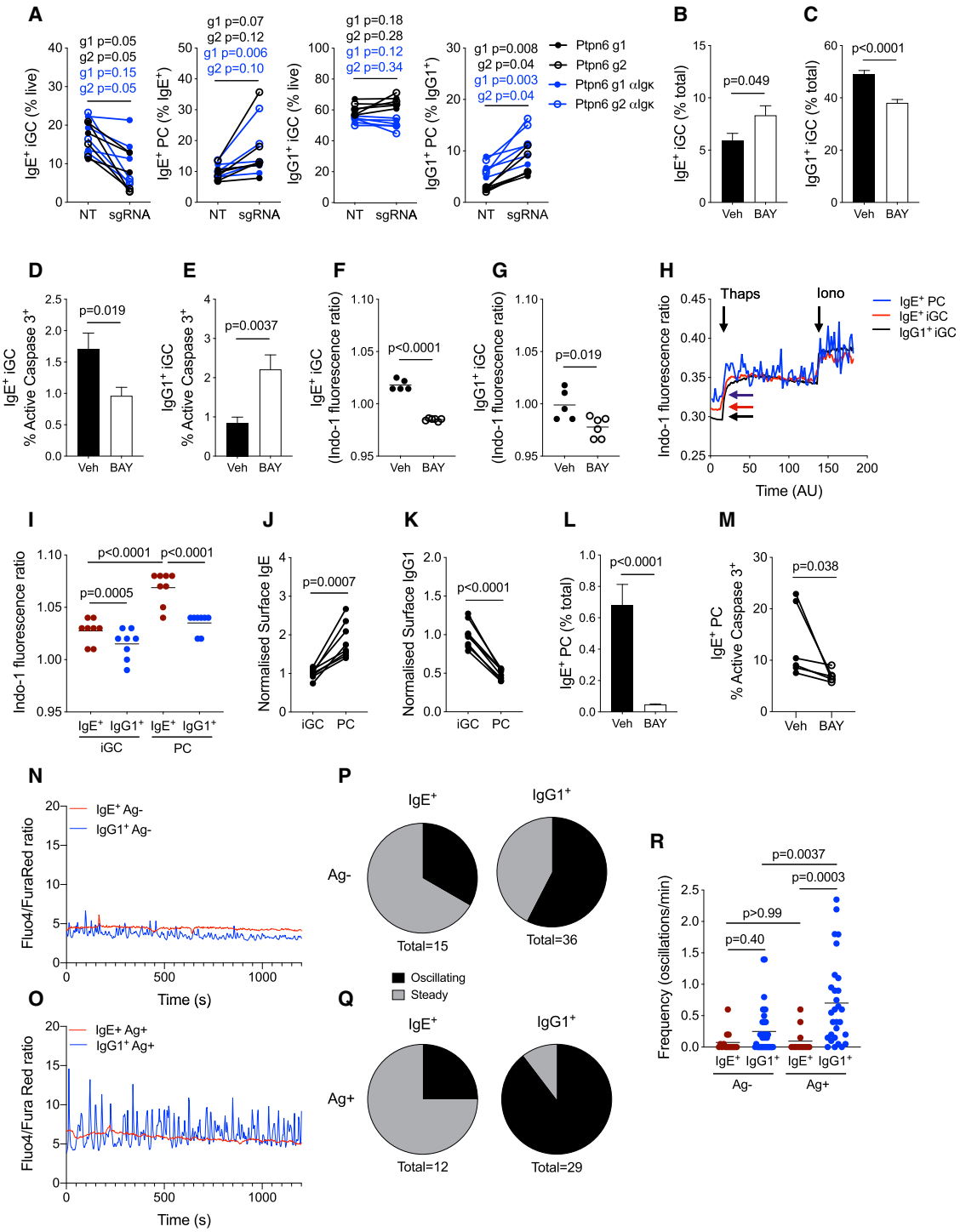

Figure 6. Calcium signaling downstream of the IgE-BCR drives apoptosis in IgE$^+$ B cells and PCs

(A) Targeting of *Ptpn6* in iGC cultures using 2 sgRNAs not present in Cherry-Brie library. sgRNA 1 and 2 (g1 and g2) shown as open and closed circles, each point represents a replicate. Conditions where 500 ng/ml anti-Igκ F(ab′)$_2$ was added for the final 2 days of culture shown in blue. Proportions of IgE$^+$ iGCs, IgE$^+$ PCs, IgG1$^+$ iGCs, and IgG1$^+$ PCs (graphs from left to right) shown for nontargeted (NT) (GFP$^+$ mCherry$^-$) and targeted (sgRNA) (GFP$^+$ mCherry$^+$) comparing cells within the same well (connected by a line). Data are pooled from three separate experiments.

(B and C) Proportions (as a % of live lymphocytes) of IgE$^+$ iGCs (B) and IgG1$^+$ iGCs (C) after cells were treated with 1 μM of the Syk inhibitor BAY 61-3606 (white bars) or vehicle control (black bars) for the final 2 days of iGC culture. n = 10–11 technical replicates pooled from four separate experiments.

(D and E) Proportions of active caspase-3$^+$ IgE$^+$ iGCs (D) and IgG1$^+$ iGCs (E) after treatment with 1 μM of the Syk inhibitor BAY 61-3606 (white bars) or vehicle control (black bars) for the final 2 days of iGC culture. n = 10–11 technical replicates pooled from the same four experiments as in (B and C).

(legend continued on next page)

types (Figure 7A), and caused loss of IgE$^+$ iGCs and IgE$^+$ PCs; however, increased apoptosis was only observed in IgE$^+$ PCs (Figures 7B and 7C), indicating that IgE$^+$ PCs are uniquely sensitized to calcium-induced apoptosis. Culturing cells with the ATP2A2 inhibitor thapsigargin resulted in a substantial loss of IgE$^+$ iGCs and IgE$^+$ PCs (Figure 7D), as well as a decrease in the proportions of IgE$^+$ iGCs and IgG1$^+$ PCs when cells were cultured with thapsigargin for longer time points (Figure S7D). This was accompanied by increased annexin V staining in IgE$^+$ iGCs and PCs (Figures 7E and S7E). Thus, IgE$^+$ PCs and, to some extent, IgE$^+$ iGCs have enhanced basal levels of intracellular calcium and are more sensitive to calcium-induced apoptosis than IgG1$^+$ B cells.

Chronic elevation of calcium levels can result in calcium overload in mitochondria, triggering cell death. MitoTracker Green staining for mitochondrial mass was slightly lower in IgE$^+$ iGCs than in IgG1$^+$ iGCs but markedly reduced in PCs (Figures S7F and S7G). Mitochondrial mass in *ex vivo* cells was also lower in IgE$^+$ PCs than in IgE$^+$ GC B cells (Figure S7H) but only mildly reduced in IgG1$^+$ PCs compared with IgG1$^+$ GC B cells (Figure S7I). Thus, differentiation of IgE$^+$ GC B cells to PCs is associated with a markedly reduced mitochondrial mass, consistent with previous findings in unswitched cells (Jang et al., 2015; Lin et al., 2015).

Rhod-2 intensity, a measure of mitochondrial calcium, correlated with mitochondrial mass (Figures S7J and S7K). However, when normalized to MitoTracker Green, Rhod-2 was the highest in IgE$^+$ PCs (Figure S7L). Blocking mitochondrial calcium uptake by Ru360 had little effect on iGCs (data not shown) but enhanced proportions of IgE$^+$ PCs and to a lesser extent IgG1$^+$ PCs differentiated without anti-Igκ F(ab′)$_2$ (Figures S7M and S7N). This was accompanied by decreased proportions of active caspase-3$^+$ IgE$^+$ PCs (Figures S7O and S7P).

To further link sensitivity to calcium-induced cell death and the mitochondrial apoptotic pathway, we tested whether the calcium-induced apoptosis depended on BCL2L11. We performed double targeting of *Bcl2l11* and *Atp2b1* (Figure 7F). As seen previously (Figure 5B), targeting *Bcl2l11* alone resulted in increased proportions of IgE$^+$ PCs, which had decreased proportions of active caspase-3$^+$ cells (Figures 7G and 7H). By contrast, targeting of *Atp2b1* resulted in decreased proportions of IgE$^+$ PCs and increased proportions of active caspase-3$^+$ cells (Figures 7G and 7H). The double-targeted population had increased proportions of the IgE$^+$ PCs, almost to the level of *Bcl2l11*-targeted cells, whereas active caspase-3$^+$ proportions were comparable to nontargeted cells (Figures 7G and 7H). Thus, elevated cytosolic calcium drives apoptosis of IgE$^+$ PCs mainly through BCL2L11.

DISCUSSION

Our study represents a genome-wide identification of genes involved in class switching, proliferation, survival, and differentiation of IgG1- and IgE-B cells. We confirmed the pathways required for tonic BCR- and BAFF-R-dependent signaling to B cell survival and for CD40- and IL-4-dependent proliferation, survival, class switching, and PC differentiation, validating the screening method. Thus, the screen data present a useful resource to investigate the mechanisms underlying class-switched B cell responses. We demonstrate their utility for studies of molecular pathways that control IgE$^+$ B cell differentiation and lifespan. The results confirm the importance of antigen-independent IgE-BCR signaling and reveal the downstream mechanisms, including previously unreported genes and pathways.

We demonstrated a role for the PI3K-mTOR signaling pathway in driving PC differentiation of IgE$^+$ B cells, extending previous data showing that the IgE-BCR autonomously induces phosphorylation of CD19 and the PI3K p85 subunit (Haniuda et al., 2016). In B cells, PI3K signaling promotes PC differentiation upstream of IRF4 (Haniuda et al., 2016; Omori et al., 2006; Sciammas et al., 2006); however, the molecular mechanisms remain unclear. Our data revealed that in IgE$^+$ cells, this molecular connection depended on mTOR's ability to promote accumulation of IRF4 protein through a post-transcriptional mechanism. As the *Irf4* gene carries a potential 5′ terminal oligopyrimidine (TOP) motif, we hypothesize that PI3K stimulates Irf4 translation via mTOR-mediated phosphorylation of EIF4EBP1 (Thoreen et al., 2012). By contrast, antigen-induced signaling through

(F and G) Indo-1 fluorescence ratios in IgE$^+$ iGCs (F) and IgG1$^+$ iGCs (G) treated with 1 μM of the Syk inhibitor BAY 61-3606 (open circles) or vehicle control (closed circles) added for the final 2 days of iGC culture. Data are pooled from two independent experiments.
(H) Baseline calcium (indicated by arrows), followed by calcium flux induced by 1 μM thapsigargin (Thaps), followed by 5 μg/ml ionomycin (Iono) in IgG1$^+$ iGCs (black line), IgE$^+$ iGCs (red line), and IgE$^+$ PCs (blue line). Calcium levels shown as Indo-1 fluorescence ratio. Data are representative of four biological replicates from independent experiments.
(I) Normalized baseline Indo-1 ratios at day 8 of iGC culture.
(J) Normalized surface IgE-BCR expression in IgE$^+$ iGCs compared with IgE$^+$ PCs.
(K) Normalized surface IgG1-BCR expression in IgG1$^+$ iGCs compared with IgG1$^+$ PCs. Cells were cultured with 500 ng/ml anti-Igκ F(ab′)$_2$ for the final 2 days of culture. In (J and K) each point represents a replicate, cells within the same well are connected by a line, data are pooled from two independent experiments.
(L) Proportions (as a % of live lymphocytes) of IgE$^+$ PCs, as described for (B–E).
(M) Proportions of active caspase-3$^+$ sorted IgE$^+$ PCs cultured with 1 μM of the Syk inhibitor BAY 61-3606 (open circles) or vehicle control (closed circles) for 20 h. Data are pooled from two independent experiments.
(N and O) Representative individual calcium traces for IgE$^+$ iGCs (red line) and IgG1$^+$ iGCs (blue line). Cells cultured without antigen (Ag$^-$) (N) or with 500 ng/ml anti-Igκ F(ab′)$_2$ (Ag$^+$) (O) for the final 2 days of iGC cultures.
(P and Q) Proportions of IgE$^+$ iGCs and IgG1$^+$ iGCs where the calcium traces were oscillating (black slice) or steady (gray slice). Cells cultured without Ag (Ag$^-$) (P) or with 500 ng/ml anti-Igκ F(ab′)$_2$ (Ag$^+$) (Q) for the final 2 days of iGC cultures. Total numbers of traces analyzed are indicated.
(R) Frequency of oscillations per minute in calcium traces from IgE$^+$ and IgG1$^+$ iGC cells cultured with and without antigen as described for (N–Q). Data in (P–R) are pooled from two separate experiments.
p values indicated using paired t test (A, J, K, and M), unpaired t test (B–G and L), one-way RM ANOVA with Sidak's multiple comparisons test (I), Kruskal-Wallis test with Dunn's multiple comparisons test (R). In (F, G, and I) each dot represents a technical replicate, in (M) each dot represents a biological replicate, in (R) each dot represents an individual cell, line represents mean. Bars indicate mean ± SEM.

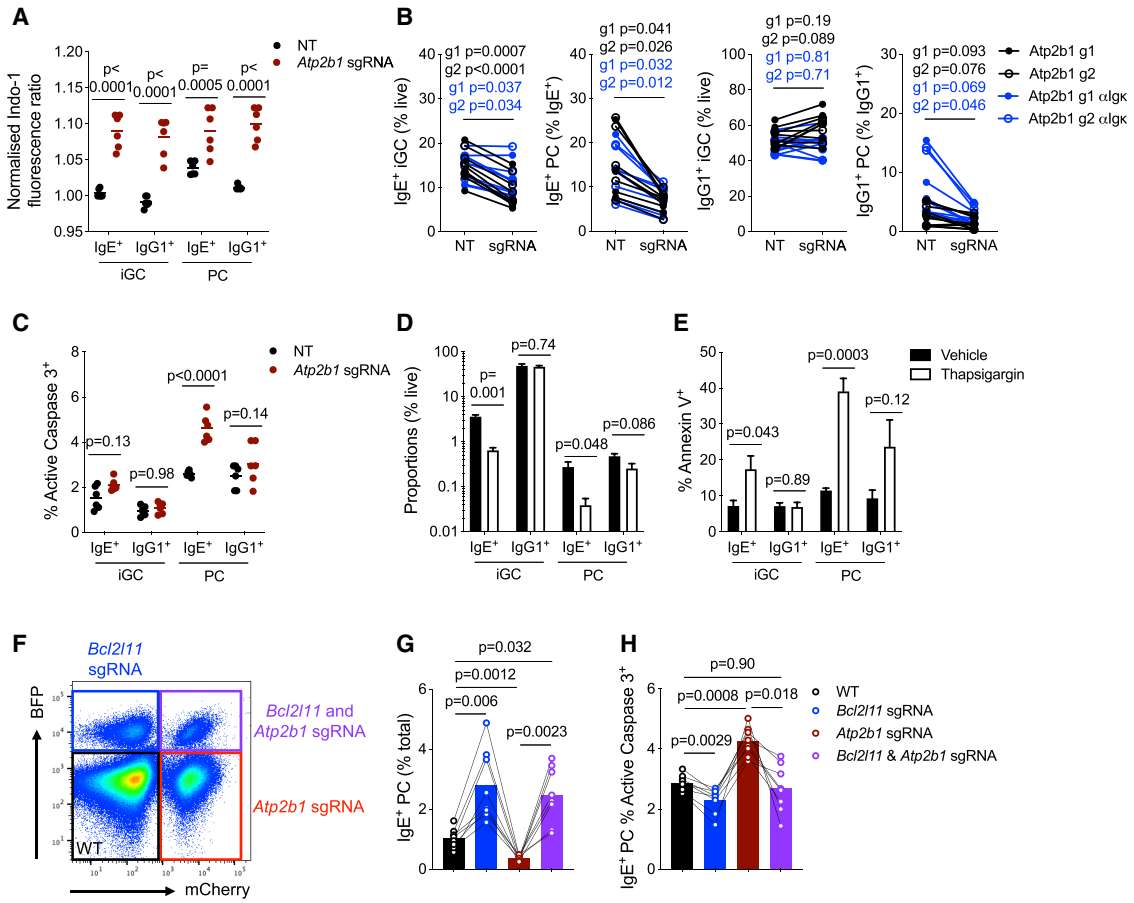

Figure 7. Elevated cytosolic calcium in IgE$^+$ B cells drives cell death through BCL2L11

(A) Normalized Indo-1 fluorescence ratio in nontargeted (black dots) and *Atp2b1*-targeted cells at day 8 of culture.

(B) Targeting of *Atp2b1* in iGC cultures using 2 sgRNAs not present in Cherry-Brie library. sgRNA 1 and 2 (g1 and g2) shown as open and closed circles, each point represents a replicate. Conditions where 500 ng/ml anti-Igκ F(ab′)$_2$ was added for the final 2 days of culture shown in blue. Proportions of IgE$^+$ iGCs, IgE$^+$ PCs, IgG1$^+$ iGCs, and IgG1$^+$ PCs (graphs from left to right) shown for nontargeted (NT) (GFP$^+$ mCherry$^-$) and targeted (sgRNA) (GFP$^+$ mCherry$^+$) comparing cells within the same well (connected by a line). Data are pooled from four separate experiments.

(C) Proportions of nontargeted (NT) (black dots) and *Atp2b1*-targeted (red dots) cells that are active caspase-3$^+$ at day 8 of iGC culture.

(D) Proportions of IgE$^+$ and IgG1$^+$ cells shown for 10 nM thapsigargin treated (white bars) compared with vehicle treated (black bars) cells, where thapsigargin was added for the final 2 days of iGC cultures. n = 3 biological replicates pooled from two independent experiments.

(E) Proportions of annexin V$^+$ cells from iGC cultures as described for (D). n = 4 biological replicates pooled from three independent experiments.

(F) Representative flow plot showing *Bcl2l11*-targeted (BFP$^+$ mCherry$^-$), *Atp2b1*-targeted (BFP$^-$ mCherry$^+$), nontargeted (NT) (BFP$^-$ mCherry$^-$), and double-targeted (BFP$^+$ mCherry$^+$) populations from the same culture well.

(G) Proportion of IgE$^+$ PCs in populations described in (F) comparing cells within the same well (connected by a line).

(H) Proportion of active caspase-3$^+$ IgE$^+$ PCs in populations described in (F) comparing cells within the same well (connected by a line). In (G and H), n = 8 technical replicates pooled from two separate experiments.

p values indicated using paired t test (B), two-way RM ANOVA with Sidak's multiple comparisons test (A and C), unpaired t test (D and E), one-way RM ANOVA with Tukey's multiple comparisons test (G and H). In (A and C) each dot represents a biological replicate, line represents mean. Bars indicate mean ± SEM.

PI3K-mTOR in IgG1$^+$ cells promoted PC differentiation by activating *Irf4* transcription. Thus, the post-transcriptional regulation of IRF4 levels in IgE$^+$ cells illustrates a unique mechanism by which the IgE-BCR controls differentiation into PCs and suggests that IgE$^+$ PC differentiation depends on synergy with drivers of *Irf4* transcription, such as CD40 and IL-4R signaling.

The second key finding of our screening was the identification of calcium signaling as a negative regulator of PC differentiation and survival. This was unanticipated because intracellular calcium has long been thought to promote PC differentiation, particularly in IgG and IgE switched cells (Engels and Wienands, 2018). The calcium pathway was identified through numerous screen hits, including both early and late regulators of calcium signaling, such as *Grb2* and *Lrmp*, respectively, which regulate IgE$^+$ PCs specifically. The requirement for GRB2 in IgG1$^+$ PC may result from GRB2 potentiation of MAPK signaling (Engels et al., 2009); however, IgE$^+$ PCs were negatively regulated by GRB2. MAPK signaling may be specific downstream of the antigen-bound IgG1 receptor because it was not picked up in our IgE$^+$ PC screens. Our screens also point to a negative role for the calcineurin-NFATC3 pathway in PC differentiation, which is particularly strong in IgE$^+$ PCs. This suggests that B cell

intrinsic roles contribute to the previously identified role for NFAT proteins in inhibiting IgE and IgG1 production (Peng et al., 2001), their association with autoimmunity and allergy in genome-wide association studies (GWAS) (Ferreira et al., 2017), and enhanced allergic responses associated with elevated serum IgE levels in transplant patients treated with cyclosporin A or tacrolimus, both of which inhibit calcineurin (Asante-Korang et al., 1996; Kawamura et al., 1997). Our results recapitulate increased IgE titers observed in Ppp3r1$^{fl/fl}$ CD19$^{cre/+}$ mice immunized with NP-LPS but differ from the decreased proportions of PCs observed in these mice following intra-peritoneal immunization (Winslow et al., 2006). Therefore, the regulation of PC differentiation by PPP3R1 warrants further study, particularly given the prevalence of calcineurin inhibitors in the clinic. Furthermore, a recent forward genetic analysis in mice identified mutations in *Plcg2* and *Syk*, which resulted in augmentation of the IgE response to papain immunization (SoRelle et al., 2020). Human mutations in *PLCG2*, which attenuate calcium signaling in B cells (Wang et al., 2014), also lead to enhanced allergen-specific IgE levels in the context of phospholipase-associated antibody deficiency and immune dysregulation (Milner, 2020). Calcineurin may inhibit PC differentiation transcriptionally through the activity of NFATC3 and its target genes. The nonredundant function of NFATC3 may be explained by its requirement for a sustained calcium signal to maintain nuclear localization (Kar et al., 2016) and is also reflected by the inhibitory role of IP_3R-2, the IP_3R most sensitive to IP_3 levels (Miyakawa et al., 1999). However, since deletion of *Ppp3r1* had a stronger phenotype in IgE$^+$ cells than in IgG1$^+$ cells, which differed from that of *Nfatc3* deletion, it is possible that other PPP3R1 targets are important in the regulation of IgE$^+$ responses.

Apoptosis is suggested to limit the expansion of IgE$^+$ B cells (Haniuda et al., 2016; Oberndorfer et al., 2006); however, the importance of this pathway remains controversial (Yang et al., 2016), in part because a molecular mechanism remains to be elucidated. Our data suggest that IgE$^+$ B cell and PC death is regulated by BCR-induced ER calcium release and a balance of pro-apoptotic (BCL2L11 and BAX) and anti-apoptotic (BCL2A1D/B) proteins. This finding is mirrored by the altered expression levels of apoptotic proteins in mouse and human IgE$^+$ B cells (Ramadani et al., 2019). As has been observed previously (Haniuda et al., 2016), IgE$^+$ B cells exhibit increased basal calcium levels, which we show is further increased in IgE$^+$ PCs. Notably, the intracellular calcium levels in IgE$^+$ PCs depend on SYK, indicating that they are driven by ongoing IgE-BCR signaling. Consistently, inhibition of SYK prevents the apoptosis of isolated IgE$^+$ PCs, indicating that IgE-BCR signaling regulates their survival after differentiation. It is interesting to speculate that this mechanism arises from elevated surface expression of the IgE-BCR on these cells (He et al., 2013; Ramadani et al., 2017).

Chronic elevation of intracellular calcium downstream of the BCR leads to mitochondrial dysfunction and cell death (Akkaya et al., 2018). Mitochondrial dysfunction caused by excessive entry of calcium is itself regulated by pro- and anti-apoptotic proteins. For example, in macrophages, BAX promotes calcium flow from the ER into mitochondria, resulting in cell death (Roca et al., 2019). Conversely, BCL2 reduces mitochondrial Ca^{2+} uptake by blocking IP_3-mediated Ca^{2+} release from the ER through inhibition of IP_3Rs in a T cell line (Chen et al., 2004). We observed decreased mitochondrial mass upon PC differentiation, which was augmented in IgE$^+$ PCs. This is in line with the proposed transcriptional regulation of mitochondrial mass by IRF4 in early PCs (Low et al., 2019) and the notion that reductions in mitochondrial mass correlate with a predisposition of B cells to differentiate into PCs (Jang et al., 2015). Overall, this suggests that reduced calcium buffering by mitochondria, along with sustained calcium release from the ER, is a key mechanism by which the lifespan of IgE$^+$ PCs is limited. Indeed, although the role of apoptosis in IgE$^+$ GC B cells has been controversial, IgE$^+$ PCs have a high level of apoptosis *in vivo* and their numbers are specifically increased by overexpression of the anti-apoptotic protein BCL2 (Yang et al., 2012, 2020). Thus, BCR apoptotic signaling in IgE$^+$ PCs could be responsible for their short lifespan. Because further remodeling of mitochondria has been suggested in long-lived PCs (Low et al., 2019), it will be interesting to understand the importance of calcium signaling in regulating the survival of long-lived IgE$^+$ PCs generated after chronic allergen exposure (Asrat et al., 2020).

Overall, our genome-wide CRISPR screens indicate that the chronic dynamics of IgE-BCR signaling translates into a distinct quality of calcium signaling in IgE$^+$ B cells and contributes to curtailing IgE$^+$ PC differentiation and survival. The stringent control of the IgE$^+$ cell fates helps to explain the self-limiting nature of IgE responses and suggests that dysregulation of this pathway may contribute to allergy.

Limitations of the study

Although genome-wide CRISPR screens provide an opportunity to study individual gene effects on the fates of IgE$^+$ and IgG$^+$ B cells at a mostly unbiased and unprecedented scale, they may miss important genes due to the statistical noise inherent to the size of the experiment. Because it is currently not feasible to validate the editing of all genes in the screen, some genes may be missed due to inefficient targeting. Relevant mechanisms may also remain undetected if they are encoded by redundant genes. Therefore, additional mining of these datasets and simultaneous disruption of whole gene families may reveal additional insights.

The *in vitro* culture conditions used in this study may miss physiologically important regulation arising from interactions of IgE$^+$ B cells with other immune cells *in vivo*. Although we validated the importance of PPP3R1 and NFATC3 for the regulation of IgE$^+$ PCs numbers in mice post-immunization, the mechanisms by which the calcium pathway regulates PC differentiation and apoptosis *in vivo* require further investigation. Formally linking this pathway to allergy will similarly require dedicated *in vivo* allergy models. Finally, extrapolation of our data to human IgE responses will need to consider that unlike in the mouse, in humans the IgE-BCR exists as two membrane isoforms, which arise due to alternative splicing and may differ in their signaling.

STAR★METHODS

Detailed methods are provided in the online version of this paper and include the following:

- KEY RESOURCES TABLE
- RESOURCE AVAILABILITY

SUPPLEMENTAL INFORMATION

Supplemental information can be found online at https://doi.org/10.1016/j.immuni.2021.11.006.

ACKNOWLEDGMENTS

This work was supported by the Francis Crick Institute, which receives its core funding from the Cancer Research UK (FC001185), the UK Medical Research Council (FC001185), and the Wellcome Trust (FC001185). This research was funded in whole, or in part, by the Wellcome Trust (grant number FC001185). For the purpose of open access, the author has applied a CC BY public copyright license to any Author Accepted Manuscript version arising from this submission. We thank the Francis Crick Institute Science Technology Platforms for their help with cell sorting and next-generation sequencing and Harshil Patel from the Bioinformatics and Biostatistics Science Technology Platform at the Francis Crick Institute for performing the bioinformatics analysis of the RNA-seq data. We also thank Daisuke Kitamura for the 40LB cells and Lars Nitschke and Richard Cornall for sharing the *Grb2*$^{fl/fl}$*Cd79a*$^{cre/+}$ mice. We also thank Edina Schweighoffer and Victor Tybulewicz for providing the Brie CRISPR library and the Syk inhibitor BAY 61-3606. We thank Martin Turner for critical reading of the manuscript.

AUTHOR CONTRIBUTIONS

R.N. designed and conducted the experiments and analyzed the data, P.T. designed the experiments analyzed the data and supervised the research. R.N. and P.T. wrote the paper.

DECLARATION OF INTERESTS

The authors declare no competing interests.

Received: February 25, 2021
Revised: July 30, 2021
Accepted: November 12, 2021
Published: December 7, 2021

REFERENCES

Achatz, G., Nitschke, L., and Lamers, M.C. (1997). Effect of transmembrane and cytoplasmic domains of IgE on the IgE response. Science *276*, 409–411.

Akkaya, M., Traba, J., Roesler, A.S., Miozzo, P., Akkaya, B., Theall, B.P., Sohn, H., Pena, M., Smelkinson, M., Kabat, J., et al. (2018). Second signals rescue B cells from activation-induced mitochondrial dysfunction and death. Nat. Immunol. *19*, 871–884.

Altarejos, J.Y., and Montminy, M. (2011). CREB and the CRTC co-activators: sensors for hormonal and metabolic signals. Nat. Rev. Mol. Cell Biol. *12*, 141–151.

Asante-Korang, A., Boyle, G.J., Webber, S.A., Miller, S.A., and Fricker, F.J. (1996). Experience of FK506 immune suppression in pediatric heart transplantation: a study of long-term adverse effects. J. Heart Lung Transplant. *15*, 415–422.

Asrat, S., Kaur, N., Liu, X., Ben, L.H., Kajimura, D., Murphy, A.J., Sleeman, M.A., Limnander, A., and Orengo, J.M. (2020). Chronic allergen exposure drives accumulation of long-lived IgE plasma cells in the bone marrow, giving rise to serological memory. Sci. Immunol. *5*, eaav8402.

Canté-Barrett, K., Winslow, M.M., and Crabtree, G.R. (2007). Selective role of NFATc3 in positive selection of thymocytes. J. Immunol. *179*, 103–110.

Chen, R., Valencia, I., Zhong, F., McColl, K.S., Roderick, H.L., Bootman, M.D., Berridge, M.J., Conway, S.J., Holmes, A.B., Mignery, G.A., and Velez, P. (2004). Bcl-2 functionally interacts with inositol 1,4,5-trisphosphate receptors to regulate calcium release from the ER in response to inositol 1,4,5-trisphosphate. J. Cell Biol. *166*, 193–203.

Chen, S., Sanjana, N.E., Zheng, K., Shalem, O., Lee, K., Shi, X., Scott, D.A., Song, J., Pan, J.Q., Weissleder, R., et al. (2015). Genome-wide CRISPR screen in a mouse model of tumor growth and metastasis. Cell *160*, 1246–1260.

Crawford, G., Hayes, M.D., Seoane, R.C., Ward, S., Dalessandri, T., Lai, C., Healy, E., Kipling, D., Proby, C., Moyes, C., et al. (2018). Epithelial damage and tissue γδ T cells promote a unique tumor-protective IgE response. Nat. Immunol. *19*, 859–870.

Croote, D., Darmanis, S., Nadeau, K.C., and Quake, S.R. (2018). High-affinity allergen-specific human antibodies cloned from single IgE B cell transcriptomes. Science *362*, 1306–1309.

Dobin, A., Davis, C.A., Schlesinger, F., Drenkow, J., Zaleski, C., Jha, S., Batut, P., Chaisson, M., and Gingeras, T.R. (2013). STAR: ultrafast universal RNA-seq aligner. Bioinformatics *29*, 15–21.

Doench, J.G., Fusi, N., Sullender, M., Hegde, M., Vaimberg, E.W., Donovan, K.F., Smith, I., Tothova, Z., Wilen, C., Orchard, R., et al. (2016). Optimized sgRNA design to maximize activity and minimize off-target effects of CRISPR-Cas9. Nat. Biotechnol. *34*, 184–191.

Engels, N., König, L.M., Heemann, C., Lutz, J., Tsubata, T., Griep, S., Schrader, V., and Wienands, J. (2009). Recruitment of the cytoplasmic adaptor Grb2 to surface IgG and IgE provides antigen receptor-intrinsic costimulation to class-switched B cells. Nat. Immunol. *10*, 1018–1025.

Engels, N., and Wienands, J. (2018). Memory control by the B cell antigen receptor. Immunol. Rev. *283*, 150–160.

Erazo, A., Kutchukhidze, N., Leung, M., Christ, A.P.G., Urban, J.F., Curotto de Lafaille, M.A., and Lafaille, J.J. (2007). Unique maturation program of the IgE response *in vivo*. Immunity *26*, 191–203.

Ferreira, M.A., Vonk, J.M., Baurecht, H., Marenholz, I., Tian, C., Hoffman, J.D., Helmer, Q., Tillander, A., Ullemar, V., Van Dongen, J., et al. (2017). Shared genetic origin of asthma, hay fever and eczema elucidates allergic disease biology. Nat. Genet. *49*, 1752–1757.

Fitzsimmons, C.M., Falcone, F.H., and Dunne, D.W. (2014). Helminth allergens, parasite-specific IgE, and its protective role in human immunity. Front. Immunol. *5*, 61.

Haniuda, K., Fukao, S., Kodama, T., Hasegawa, H., and Kitamura, D. (2016). Autonomous membrane IgE signaling prevents IgE-memory formation. Nat. Immunol. *17*, 1109–1117.

Hasbold, J., Lyons, A.B., Kehry, M.R., and Hodgkin, P.D. (1998). Cell division number regulates IgG1 and IgE switching of B cells following stimulation by CD40 ligand and IL-4. Eur. J. Immunol. *28*, 1040–1051.

He, J.S., Meyer-Hermann, M., Xiangying, D., Zuan, L.Y., Jones, L.A., Ramakrishna, L., de Vries, V.C.D., Dolpady, J., Aina, H., Joseph, S., et al.

(2013). The distinctive germinal center phase of IgE+ B lymphocytes limits their contribution to the classical memory response. J. Exp. Med. *210*, 2755–2771.

Hikida, M., Casola, S., Takahashi, N., Kaji, T., Takemori, T., Rajewsky, K., and Kurosaki, T. (2009). PLC-γ 2 is essential for formation and maintenance of memory B cells. J. Exp. Med. *206*, 681–689.

Hobeika, E., Thiemann, S., Storch, B., Jumaa, H., Nielsen, P.J., Pelanda, R., and Reth, M. (2006). Testing gene function early in the B cell lineage in mb1-cre mice. Proc. Natl. Acad. Sci. USA *103*, 13789–13794.

Jang, K.-J., Mano, H., Aoki, K., Hayashi, T., Muto, A., Nambu, Y., Takahashi, K., Itoh, K., Taketani, S., Nutt, S.L., et al. (2015). Mitochondrial function provides instructive signals for activation-induced B-cell fates. Nat. Commun. *6*, 6750.

Kar, P., Mirams, G.R., Christian, H.C., and Parekh, A.B. (2016). Control of NFAT isoform activation and NFAT-dependent gene expression through two coincident and spatially segregated intracellular Ca2+ signals. Mol. Cell *64*, 746–759.

Kawamura, N., Furuta, H., Tame, A., Kobayashi, I., Ariga, T., Okano, M., and Sakiyama, Y. (1997). Extremely high serum level of IgE during immunosuppressive therapy: paradoxical effect of cyclosporine A and tacrolimus. Int. Arch. Allergy Immunol. *112*, 422–424.

Kersey, P.J., Allen, J.E., Armean, I., Boddu, S., Bolt, B.J., Carvalho-Silva, D., Christensen, M., Davis, P., Falin, L.J., Grabmueller, C., et al. (2016). Ensembl Genomes 2016: more genomes, more complexity. Nucleic Acids Res *44*, D574–D580.

Kräutler, N.J., Suan, D., Butt, D., Bourne, K., Hermes, J.R., Chan, T.D., Sundling, C., Kaplan, W., Schofield, P., Jackson, J., et al. (2017). Differentiation of germinal center B cells into plasma cells is initiated by high-affinity antigen and completed by Tfh cells. J. Exp. Med. *214*, 1259–1267.

Laffleur, B., Duchez, S., Tarte, K., Denis-Lagache, N., Péron, S., Carrion, C., Denizot, Y., and Cogné, M. (2015). Self-restrained B cells arise following membrane IgE expression. Cell Rep *10*, 900–909.

Lewandoski, M., Meyers, E.N., and Martin, G.R. (1997). Analysis of FGF8 gene function in vertebrate development. Cold Spring Harb. Symp. Quant. Biol. *62*, 159–168.

Li, B., and Dewey, C.N. (2011). RSEM: accurate transcript quantification from RNA-Seq data with or without a reference genome. BMC Bioinformatics *12*, 323.

Li, S., Yen, L., Pastor, W.A., Johnston, J.B., Du, J., Shew, C.J., Liu, W., Ho, J., Stender, B., Clark, A.T., et al. (2016). Mouse MORC3 is a GHKL ATPase that localizes to H3K4me3 marked chromatin. Proc. Natl. Acad. Sci. USA *113*, E5108–E5116.

Li, W., Xu, H., Xiao, T., Cong, L., Love, M.I., Zhang, F., Irizarry, R.A., Liu, J.S., Brown, M., and Liu, X.S. (2014). MAGeCK enables robust identification of essential genes from genome-scale CRISPR-Cas9 knockout screens. Genome Biol *15*, 554.

Lin, W.H.W., Adams, W.C.C., Nish, S.A.A., Chen, Y.H., Yen, B., Rothman, N.J.J., Kratchmarov, R., Okada, T., Klein, U., and Reiner, S.L.L. (2015). Asymmetric PI3K signaling driving developmental and regenerative cell fate bifurcation. Cell Rep *13*, 2203–2218.

Liu, W., Chen, E., Zhao, X.W., Wan, Z.P., Gao, Y.R., Davey, A., Huang, E., Zhang, L., Crocetti, J., Sandoval, G., et al. (2012). The scaffolding protein synapse-associated protein 97 is required for enhanced signaling through isotype-switched IgG memory B cell receptors. Sci. Signal. *5*, ra54.

Love, M.I., Huber, W., and Anders, S. (2014). Moderated estimation of fold change and dispersion for RNA-seq data with DESeq2. Genome Biol *15*, 550.

Low, M.S.Y., Brodie, E.J., Fedele, P.L., Liao, Y., Grigoriadis, G., Strasser, A., Kallies, A., Willis, S.N., Tellier, J., Shi, W., et al. (2019). IRF4 activity is required in established plasma cells to regulate gene transcription and mitochondrial homeostasis. Cell Rep *29*, 2634–2645, e5.

Marichal, T., Starkl, P., Reber, L.L., Kalesnikoff, J., Oettgen, H.C., Tsai, M., Metz, M., and Galli, S.J. (2013). A beneficial role for immunoglobulin E in host defense against honeybee venom. Immunity *39*, 963–975.

Martin, M. (2011). CUTADAPT removes adapter sequences from high-throughput sequencing reads. EMBnet.journal *17*, 10–12.

Milner, J.D. (2020). Primary atopic disorders. Annu. Rev. Immunol. *38*, 785–808.

Miyakawa, T., Maeda, A., Yamazawa, T., Hirose, K., Kurosaki, T., and Iino, M. (1999). Encoding of Ca2+ signals by differential expression of IP3 receptor subtypes. EMBO J *18*, 1303–1308.

Neilson, J.R., Winslow, M.M., Hur, E.M., and Crabtree, G.R. (2004). Calcineurin B1 is essential for positive but not negative selection during thymocyte development. Immunity *20*, 255–266.

Nojima, T., Haniuda, K., Moutai, T., Matsudaira, M., Mizokawa, S., Shiratori, I., Azuma, T., and Kitamura, D. (2011). *In-vitro* derived germinal centre B cells differentially generate memory B or plasma cells *in vivo*. Nat. Commun. *2*, 465.

Nowosad, C.R., Spillane, K.M., and Tolar, P. (2016). Germinal center B cells recognize antigen through a specialized immune synapse architecture. Nat. Immunol. *17*, 870–877.

Oberndorfer, I., Schmid, D., Geisberger, R., Achatz-Straussberger, G., Crameri, R., Lamers, M., and Achatz, G. (2006). HS1-associated protein X-1 interacts with membrane-bound IgE: impact on receptor-mediated internalization. J. Immunol. *177*, 1139–1145.

Omori, S.A., Cato, M.H., Anzelon-Mills, A., Puri, K.D., Shapiro-Shelef, M., Calame, K., and Rickert, R.C. (2006). Regulation of class-switch recombination and plasma cell differentiation by phosphatidylinositol 3-kinase signaling. Immunity *25*, 545–557.

Park, J., Lim, K., Kim, J.S., and Bae, S. (2017). Cas-analyzer: an online tool for assessing genome editing results using NGS data. Bioinformatics *33*, 286–288.

Pawankar, R. (2014). Allergic diseases and asthma: a global public health concern and a call to action. World Allergy Organ. J. *7*, 12.

Peng, S.L., Gerth, A.J., Ranger, A.M., and Glimcher, L.H. (2001). NFATc1 and NFATc2 together control both T and B cell activation and differentiation. Immunity *14*, 13–20.

Phan, T.G., Amesbury, M., Gardam, S., Crosbie, J., Hasbold, J., Hodgkin, P.D., Basten, A., and Brink, R. (2003). B cell receptor-independent stimuli trigger immunoglobulin (Ig) class switch recombination and production of IgG autoantibodies by anergic self-reactive B cells. J. Exp. Med. *197*, 845–860.

Phan, T.G., Paus, D., Chan, T.D., Turner, M.L., Nutt, S.L., Basten, A., and Brink, R. (2006). High affinity germinal center B cells are actively selected into the plasma cell compartment. J. Exp. Med. *203*, 2419–2424.

Platt, R.J., Chen, S., Zhou, Y., Yim, M.J., Swiech, L., Kempton, H.R., Dahlman, J.E., Parnas, O., Eisenhaure, T.M., Jovanovic, M., et al. (2014). CRISPR-Cas9 knockin mice for genome editing and cancer modeling. Cell *159*, 440–455.

R Development Core Team. (2015). R: a language and environment for statistical computing (R Foundation for Statistical Computing). http://www.r-project.org/.

Ramadani, F., Bowen, H., Gould, H.J., and Fear, D.J. (2019). Transcriptional analysis of the human IgE-expressing plasma cell differentiation pathway. Front. Immunol. *10*, 402.

Ramadani, F., Bowen, H., Upton, N., Hobson, P.S., Chan, Y.C., Chen, J.B., Chang, T.W., McDonnell, J.M., Sutton, B.J., Fear, D.J., and Gould, H.J. (2017). Ontogeny of human IgE-expressing B cells and plasma cells. Allergy *72*, 66–76.

Roca, F.J., Whitworth, L.J., Redmond, S., Jones, A.A., and Ramakrishnan, L. (2019). TNF induces pathogenic programmed macrophage necrosis in tuberculosis through a mitochondrial-lysosomal-endoplasmic reticulum circuit. Cell *178*, 1344–1361, e11.

Sanjana, N.E., Shalem, O., and Zhang, F. (2014). Improved vectors and genome-wide libraries for CRISPR screening. Nat. Methods *11*, 783–784.

Satpathy, S., Wagner, S.A., Beli, P., Gupta, R., Kristiansen, T.A., Malinova, D., Francavilla, C., Tolar, P., Bishop, G.A., Hostager, B.S., and Choudhary, C. (2015). Systems-wide analysis of BCR signalosomes and downstream phosphorylation and ubiquitylation. Mol. Syst. Biol. *11*, 810.

Schindelin, J., Arganda-Carreras, I., Frise, E., Kaynig, V., Longair, M., Pietzsch, T., Preibisch, S., Rueden, C., Saalfeld, S., Schmid, B., et al. (2012). Fiji: an open-source platform for biological-image analysis. Nat. Methods *9*, 676–682.

Schmitt, M.E.R., Lutz, J., Haase, P., Bösl, M.R., Wienands, J., Engels, N., and Voehringer, D. (2020). The B-cell antigen receptor of IgE-switched plasma cells regulates memory IgE responses. J. Allergy Clin. Immunol. *146*, 642–651, e5.

Sciammas, R., Shaffer, A.L., Schatz, J.H., Zhao, H., Staudt, L.M., and Singh, H. (2006). Graded expression of interferon regulatory Factor-4 coordinates isotype switching with plasma cell differentiation. Immunity *25*, 225–236.

Shindo, Y., Kim, M.R., Miura, H., Yuuki, T., Kanda, T., Hino, A., and Kusakabe, Y. (2010). Lrmp/Jaw1 is expressed in sweet, bitter, and umami receptor-expressing cells. Chem. Senses *35*, 171–177.

Soneoka, Y., Cannon, P.M., Ramsdale, E.E., Griffiths, J.C., Romano, G., Kingsman, S.M., and Kingsman, A.J. (1995). A transient three-plasmid expression system for the production of high titer retroviral vectors. Nucleic Acids Res *23*, 628–633.

SoRelle, J.A., Chen, Z., Wang, J., Yue, T., Choi, J.H., Wang, K.-W., Zhong, X., Hildebrand, S., Russell, J., Scott, L., et al. (2020). Dominant atopy risk mutations identified by mouse forward genetic analysis. Allergy *76*, 1095–1108.

Spanopoulou, E., Roman, C.A.J., Corcoran, L.M., Schlissel, M.S., Silver, D.P., Nemazee, D., Nussenzweig, M.C., Shinton, S.A., Hardy, R.R., and Baltimore, D. (1994). Functional immunoglobulin transgenes guide ordered B-cell differentiation in Rag-1-deficient mice. Genes Dev *8*, 1030–1042.

Starkl, P., Marichal, T., Gaudenzio, N., Reber, L.L., Sibilano, R., Tsai, M., and Galli, S.J. (2016). IgE antibodies, FcεRIα, and IgE-mediated local anaphylaxis can limit snake venom toxicity. J. Allergy Clin. Immunol. *137*, 246–257, e11.

Szklarczyk, D., Gable, A.L., Lyon, D., Junge, A., Wyder, S., Huerta-Cepas, J., Simonovic, M., Doncheva, N.T., Morris, J.H., Bork, P., et al. (2019). STRING v11: protein-protein association networks with increased coverage, supporting functional discovery in genome-wide experimental datasets. Nucleic Acids Res *47*, D607–D613.

Thoreen, C.C., Chantranupong, L., Keys, H.R., Wang, T., Gray, N.S., and Sabatini, D.M. (2012). A unifying model for mTORC1-mediated regulation of mRNA translation. Nature *485*, 109–113.

Wang, J., Sohn, H., Sun, G., Milner, J.D., and Pierce, S.K. (2014). The autoinhibitory C-terminal SH2 domain of phospholipase C-γ2 stabilizes B cell receptor signalosome assembly. Sci. Signal. *7*, ra89.

Wang, T., Birsoy, K., Hughes, N.W., Krupczak, K.M., Post, Y., Wei, J.J., Lander, E.S., and Sabatini, D.M. (2015). Identification and characterization of essential genes in the human genome. Science *350*, 1096–1101.

Wang, T., Lander, E.S., and Sabatini, D.M. (2016). Single guide RNA library design and construction. Cold Spring Harb. Protoc. 2016, pdb.prot090803.

Winslow, M.M., Gallo, E.M., Neilson, J.R., and Crabtree, G.R. (2006). The calcineurin phosphatase complex modulates immunogenic B cell responses. Immunity *24*, 141–152.

Yang, Z., Robinson, M.J., Chen, X., Smith, G.A., Taunton, J., Liu, W., and Allen, C.D.C. (2016). Regulation of B cell fate by chronic activity of the IgE B cell receptor. Elife *5*, e21238.

Yang, Z., Sullivan, B.M., and Allen, C.D.C. (2012). Fluorescent *in vivo* detection reveals that IgE(+) B cells are restrained by an intrinsic cell fate predisposition. Immunity *36*, 857–872.

Yang, Z., Wu, C.M., Targ, S., and Allen, C.D.C. (2020). IL-21 is a broad negative regulator of IgE class switch recombination in mouse and human B cells. J. Exp. Med. *217*, e20190472.

STAR★METHODS

KEY RESOURCES TABLE

REAGENT or RESOURCE	SOURCE	IDENTIFIER
Antibodies		
Active Caspase 3-PE (Rabbit IgG)	BD Biosciences	Cat# 561011; RRID: AB_2033931
B220/CD45R-BV605 (Rat IgG2a, κ)	Biolegend	Cat# 103243; RRID: AB_11203907
B220/CD45R-APC (Rat IgG2a, κ)	ThermoFisher	Cat# 17-0452-83; RRID: AB_469396
B220/CD45R-PerCP Cy5.5 (Rat IgG2a, κ)	BD Biosciences	Cat# 552771; RRID: AB_394457
B220/CD45R-BUV737 (Rat IgG2a, κ)	BD Biosciences	Cat# 564449; RRID: AB_2738813
Bim-Unconjugated (Rabbit)	Abcam	Cat# Ab32158; RRID: AB_725697
Blimp1-AF647 (Rat IgG2a, κ)	Biolegend	Cat# 150003; RRID: AB_2565617
CD138-BV786 (Rat IgG2a, κ)	BD Biosciences	Cat# 740880; RRID: AB_2740530
CD138-PE (Rat IgG2a, κ)	BD Biosciences	Cat# 561070 RRID:AB_2033998
CD19-PE (Rat IgG2a, κ)	ThermoFisher	Cat# 12-0193-83; RRID: AB_657660
CD19-BV421 (Rat IgG2a, κ)	Biolegend	Cat# 115549; RRID: AB_2563066
CD19-APC (Rat IgG2a, κ)	ThermoFisher	Cat# 17-0193-80; RRID:AB_1659678
CD21/35-ef450 (Rat IgG2a, λ)	ThermoFisher	Cat# 48-0212-80 RRID: AB_2016634
CD22.2-PE (Mouse IgG1, κ)	BD Biosciences	Cat# 553384; RRID: AB_2295739
CD23-Bio (Rat IgG2a, κ)	BD Biosciences	Cat# 553137; RRID: AB_394652
CD23-PE (Rat IgG2a, κ)	BD Biosciences	Cat# 553139; RRID: AB_394654
CD38-PerCP Cy5.5 (Rat IgG2a, κ)	Biolegend	Cat# 102722; RRID: AB_2563333
CD4-BV605 (Rat IgG2a, κ)	Biolegend	Cat# 100547; RRID: AB_11125962
CD93-APC (Rat IgG2b, κ)	ThermoFisher	Cat# 17-5892-83; RRID: AB_469467
CD95/Fas-BV421 (Armenian Hamster IgG2, λ2)	BD Biosciences	Cat# 562633; RRID: AB_2737690
IgD-PE (Rat IgG2a, κ)	ThermoFisher	Cat# 12-5993-83; RRID: AB_466114
IgG1-PE Cy7 (Rat IgG)	Biolegend	Cat# 406614; RRID: AB_2562002
IgG1-APC (Rat IgG2, κ)	BD Biosciences	Cat# 550874; RRID: AB_398470
AffiniPure Fab fragment IgG-AF488	Jackson Immunoresearch Europe Ltd	Cat# 315-547-003; RRID: AB_2340223

(*Continued on next page*)

Continued

REAGENT or RESOURCE	SOURCE	IDENTIFIER
IgM-PerCP Cy5.5 (Rat IgG2a, κ)	BD Biosciences	Cat# 550881; RRID: AB_393944
IgM-PE Cy7 (Rat IgG2a, κ)	ThermoFisher	Cat# 25-5790-81; RRID: AB_469654
IgE-Bio (Rat IgG1, κ)	Biolegend	Cat# 406904; RRID: AB_315075
IgE-FITC (Rat IgG1, κ)	Biolegend	Cat# 406906; RRID: AB_493289
Purified anti-mouse IgE (Rat IgG1, κ)	Biolegend	Cat# 406902; RRID: AB_315073
IgE Fab fragment (produced from purified anti-mouse IgE)	This paper	N/A
Irf4-PerCP ef710 (Rat IgG1, κ)	ThermoFisher	Cat# 46-9858-80; RRID: AB_2573911
Phospho-S6 (Ser235/236)-AF647 (Rabbit IgG)	Cell Signaling Technology	Cat# 4851; RRID: AB_10695457
Phospho-mTOR (Ser2448)-unconjugated (Rabbit IgG)	Cell Signaling Technology	Cat# 5536; RRID: AB_10691552
TCRβ-PE (Armenian Hamster IgG2, λ2)	BD Biosciences	Cat# 553171; RRID: AB_394683
TCRβ-ef450 (Armenian Hamster IgG)	ThermoFisher	Cat# 48-5961-80; RRID: AB_11062012
Goat F(ab')$_2$ Anti-Mouse Kappa-UNLB	Southern Biotech	Cat# 1052-01; RRID: AB_2794386
Goat-anti-Rabbit-AF647	ThermoFisher	Cat# A21244; RRID: AB_2535812
PE-Mouse IgG1, κ Isotype Control	BD Biosciences	Cat# 550617; RRID: AB_10050483
Bacterial Strains		
NEB Stable Competent E.coli (High efficiency)	New England Biolabs	C3060I
Endura Electrocompetent cells	Lucigen	60242-2
Chemicals, peptides and recombinant proteins		
Ru360	Calbiochem	557440-500
Rapamycin	Calbiochem	553210
BAY61-3606	Calbiochem	574714
Thapsigargin	Calbiochem	586005
Recombinant murine IL-4	Peprotech	214-14
Recombinant murine SCF	Peprotech	250-03
Recombinant murine IL-3	Peprotech	213-13
Recombinant human IL-6	Peprotech	200-06
Recombinant murine TPO	Peprotech	315-14
Recombinant murine Flt3-ligand	Peprotech	250-31L
TransIT-LT1 Transfection Reagent	Mirus Bio LLC	MIR 2306
Polybrene	Millipore	TR-1003-G
Ionomycin Calcium salt from *Streptomyces conglobatus*	Sigma-Aldrich	IO634
NP-CGG (Chicken Gamma Globulin)	2B Scientific	N-5055E-5
Imject Alum Adjuvant	ThermoFisher	77161
Fast AP	Thermo Scientific	EF0651
Esp3I (BsmBI)	Thermo Scientific	ER0452

(*Continued on next page*)

Continued

REAGENT or RESOURCE	SOURCE	IDENTIFIER
Quick ligase	New England Biolabs	M220L
Phusion Flash High-Fidelity PCR Master Mix	ThermoFisher	F548S
Dynabeads Protein G for Immunoprecipitation	ThermoFisher	10009D
Poly-L-lysine solution	Sigma-Aldrich	P4707
Pluronic F-127 (20% Solution in DMSO)	ThermoFisher	P3000MP
Mouse BD Fc Block (2.4G2)	BD Biosciences	553141
Streptavidin-PE Cy7	ThermoFisher	25-4317-82
Streptavidin-BV421	Biolegend	405225
Streptavidin-BUV736	BD Biosciences	564293
Critical commmercial assays		
CD43 (Ly-48) MicroBeads	Miltenyi Biotech	130-049-801
Feeder Removal MicroBeads, mouse	Miltenyi Biotech	130-095-531
CD117 MicroBeads, mouse	Miltenyi Biotech	130-091-224
RNeasy Mini Kit	Qiagen	74106
RNeasy Micro Kit	Qiagen	74004
DNeasy Blood and Tissue Kit	Qiagen	69506
QuantiTect Reverse Transcription Kit	Qiagen	205311
Zyppy Plasmid Miniprep Kit	Zymo Research	D4020
Zymoclean Gel DNA Recovery Kit	Zymo Research	D4001
GeneJet Plasmid Midiprep Kit	ThermoFisher	K0481
HiSpeed Plasmid Midi Kit	Qiagen	12643
HiSpeed Plasmid Maxi Kit	Qiagen	12663
Gibson Assembly Master Mix	New England Biolabs	M5510AA
Pierce Fab Micro Preparation Kit	ThermoFisher	44685
Cy5 Mono-Reactive Dye Pack	Amersham	PA25001
Alexa Fluor™ 405 NHS Ester (Succinimidyl Ester)	ThermoFisher	A30000
eBioscience FoxP3/Transcription Factor Staining Buffer Set	ThermoFisher	00-5523-00
True-Nuclear Transcription Factor Staining Buffer Set	Biolegend	424401
BD Cytofix/Cytoperm	BD Biosciences	554714
Fixable Viability Dye	ThermoFisher	65-0865-14
MitoTracker™ Green FM	ThermoFisher	M7514
MitoTracker™ Orange CMTM Ros	ThermoFisher	M7510
Rhod-2, AM	ThermoFisher	R1245MP
TMRM	AAT Bioquest	22221
Annexin V apoptosis detection set (PE Cy7)	ThermoFisher	88-8103-74
Indo-1, AM	ThermoFisher	I1223
Fluo-4, AM	ThermoFisher	F14201
FuraRed™, AM	ThermoFisher	F3021
Mm01277042_m1 (Mouse Tbp Taqman Gene Expression Assay)	ThermoFisher	4331182
Mm03024075_m1 (Mouse Hprt Taqman Gene Expression Assay)	ThermoFisher	4331182
Mm00516431_m1 (Mouse Irf4 Taqman Gene Expression Assay)	ThermoFisher	4331182
KAPA mRNA HyperPrep Kit	Roche	KK8581
Cell Trace Violet Proliferation Kit	ThermoFisher	C43557

(*Continued on next page*)

Continued

REAGENT or RESOURCE	SOURCE	IDENTIFIER
Deposited data		
RNAseq data of 40LB culture	This paper	GSE166853
CRISPR Screen data	This paper	Table S1
Experimental models: Cell lines		
293T cells	ECACC	Cat# 12022001 RRID:CVCL_0063
40LB cells	(Nojima et al., 2011)	RRID:CVCL_A6ZS
Experimental models: Organisms/strains		
Cas9-GFP: Gt(ROSA) 26Sor$^{tm1.1(CAG-cas9*,-EGFP)Fezh}$	The Jackson Laboratory	RRID:IMSR_JAX: 024858
Grb2$^{fl/fl}$: B6.C(Cg)-*Grb2*$^{tm1.1Lnit}$/J	The Jackson Laboratory	RRID:IMSR_JAX: 020422
Cd79a$^{cre/+}$: C(Cg)-Cd79a$^{tm1(cre)Reth}$/EhobJ	The Jackson Laboratory	RRID:IMSR_JAX: 029412
RAG-1 KO: B6.129S7-*Rag1*^{tm1Mom}/J	The Jackson Laboratory	RRID:IMSR_JAX: 002216
RAG-1 KO: Rag1^{tm1Bal}	(Spanopoulou et al., 1994)	MGI:2448994; RRID: MGI:3582305
Oligonucleotides		
P5_0nt_spacer: AATGATACGGCGACCACCGAGATCTAC ACTCTTTCCCTACACGACGCTCTTCCG ATCTTTGTGGAAAGGACGAAACACCG	Broad Institute Protocols	https://portals.broadinstitute.org/gpp/public/
P5_1nt_spacer: AATGATACGGCGACCACCGAGATCTAC ACTCTTTCCCTACACGACGCTCTTCCG ATCTCTTGTGGAAAGGACGAAACACCG	Broad Institute Protocols	https://portals.broadinstitute.org/gpp/public/
P5_2nt_spacer: AATGATACGGCGACCACCGAGATCTAC ACTCTTTCCCTACACGACGCTCTTCCGA TCTGCTTGTGGAAAGGACGAAACACCG	Broad Institute Protocols	https://portals.broadinstitute.org/gpp/public/
P5_3nt_spacer: AATGATACGGCGACCACCGAGATCTAC ACTCTTTCCCTACACGACGCTCTTCCGA TCTAGCTTGTGGAAAGGACGAAACACCG	Broad Institute Protocols	https://portals.broadinstitute.org/gpp/public/
P5_4nt_spacer: AATGATACGGCGACCACCGAGATCTACA CTCTTTCCCTACACGACGCTCTTCCGAT CTCAACTTGTGGAAAGGACGAAACACCG	Broad Institute Protocols	https://portals.broadinstitute.org/gpp/public/
P5_6nt_spacer: AATGATACGGCGACCACCGAGATCTAC ACTCTTTCCCTACACGACGCTCTTCCGA TCTTGCACCTTGTGGAAAGGACGAAA CACCG	Broad Institute Protocols	https://portals.broadinstitute.org/gpp/public/
P6_7nt_spacer: AATGATACGGCGACCACCGAGATCTA CACTCTTTCCCTACACGACGCTCTTCC GATCTACGCAACTTGTGGAAAGGACGA AACACCG	Broad Institute Protocols	https://portals.broadinstitute.org/gpp/public/
P7_8nt_spacer: AATGATACGGCGACCACCGAGATCT ACACTCTTTCCCTACACGACGCTCTT CCGATCTGAAGACCCTTGTGGAAAG GACGAAACACCG	Broad Institute Protocols	https://portals.broadinstitute.org/gpp/public/
P7_A01: CAAGCAGAAGACGGCATACGAGAT CGGTTCAAGTGACTGGAGTTCAGA CGTGTGCTCTTCCGATCTTCTACT ATTCTTTCCCCTGCACTGT	Broad Institute Protocols	https://portals.broadinstitute.org/gpp/public/

(*Continued on next page*)

Continued

REAGENT or RESOURCE	SOURCE	IDENTIFIER
P7_A02: CAAGCAGAAGACGGCATACGAGA TGCTGGATTGTGACTGGAGTTCAG ACGTGTGCTCTTCCGATCTTCTAC TATTCTTTCCCCTGCACTGT	Broad Institute Protocols	https://portals.broadinstitute.org/gpp/public/
P7_A03: CAAGCAGAAGACGGCATACGAGA TTAACTCGGGTGACTGGAGTTCA GACGTGTGCTCTTCCGATCTTCTA CTATTCTTTCCCCTGCACTGT	Broad Institute Protocols	https://portals.broadinstitute.org/gpp/public/
P7_A04: CAAGCAGAAGACGGCATACGAG ATTAACAGTTGTGACTGGAGTTC AGACGTGTGCTCTTCCGATCTTC TACTATTCTTTCCCCTGCACTGT	Broad Institute Protocols	https://portals.broadinstitute.org/gpp/public/
P7_A05: CAAGCAGAAGACGGCATACGAG ATATACTCAAGTGACTGGAGTTC AGACGTGTGCTCTTCCGATCTTC TACTATTCTTTCCCCTGCACTGT	Broad Institute Protocols	https://portals.broadinstitute.org/gpp/public/
P7_A06: CAAGCAGAAGACGGCATACGAG ATGCTGAGAAGTGACTGGAGTT CAGACGTGTGCTCTTCCGATCTT CTACTATTCTTTCCCCTGCACTGT	Broad Institute Protocols	https://portals.broadinstitute.org/gpp/public/
LentiGuide_PCR1_fwd: CCCGAGGGGACCCAGAGAG	(Chen et al., 2015)	N/A
LentiGuide_Cherry_PCR1_rev: CTTGGAGCCGTACATGAACTGAGG	This paper	N/A
Library_gibson_fwd: GGCTTTATATATCTTGTGGAAAGG ACGAAACACCG	(Wang et al., 2016)	N/A
Library_gibson_rev: CTAGCCTTATTTTAACTTGCTATTT CTAGCTCTAAAAC	(Wang et al., 2016)	N/A
Irf4_g1_Amplicon _fwd: TCGTCGGCAGCGTCAGATGTGTAT AAGAGACAGGGTTCATAACTACA TGATGCCAC	This paper	N/A
Irf4_g1_Amplicon _rev: GTCTCGTGGGCTCGGAGATGTGTA TAAGAGACAGAGCTTCATATGATG TGTCTCTGG	This paper	N/A
Irf4_g2_Amplicon _fwd: TCGTCGGCAGCGTCAGATGTGTAT AAGAGACAGCCGACAGTGGTTGA TCGAC	This paper	N/A
Irf4_g2_Amplicon _rev: GTCTCGTGGGCTCGGAGATGTGT ATAAGAGACAGGCTCTGGCCTCC TCCTTG	This paper	N/A
Prdm1_g1_Amplicon _fwd: TCGTCGGCAGCGTCAGATGTGTA TAAGAGACAGCATTCCTTCTTAC AATGCTCAC	This paper	N/A

(*Continued on next page*)

Continued

REAGENT or RESOURCE	SOURCE	IDENTIFIER
Prdm1_g1_Amplicon _rev: GTCTCGTGGGCTCGGAGATGTGT ATAAGAGACAGGATAAGCACCTC TTTGGG	This paper	N/A
Prdm1_g2_Amplicon _fwd: TCGTCGGCAGCGTCAGATGTGTA TAAGAGACAGGACATGGATGGC TTTCG	This paper	N/A
Prdm1_g2_Amplicon _rev: GTCTCGTGGGCTCGGAGATGTG TATAAGAGACAGCAGGGGTGAC ACCGTGTTT	This paper	N/A
Cd22_g1_Amplicon _fwd: TCGTCGGCAGCGTCAGATGTGT ATAAGAGACAGCAATGGACATC CAGCTTAGCT	This paper	N/A
Cd22_g1_Amplicon _rev: GTCTCGTGGGCTCGGAGATGT GTATAAGAGACAGTGAAGAGGG ACAGTCAGTAGAGC	This paper	N/A
Cd22_g2_Amplicon _fwd: TCGTCGGCAGCGTCAGATGTGT ATAAGAGACAGTCTGAGCTGTA CCTTTCTAAGCAAG	This paper	N/A
Cd22_g2_Amplicon _rev: GTCTCGTGGGCTCGGAGATGT GTATAAGAGACAGCACCTTGGC TGTTTGCTC	This paper	N/A
Recombinant DNA		
Plasmid Mouse sgRNA library Brie in lentiCRISPRv2	(Doench et al., 2016)	RRID: Addgene_73632
Plasmid lentiGuide-Puro	(Sanjana et al., 2014)	RRID: Addgene_52963
Plasmid lentiGuide-Cherry	This paper	RRID: Addgene_170510
Plasmid Mouse sgRNA library Brie in lentiGuide-Cherry (Cherry Brie Library)	This paper	RRID: Addgene_170511
Plasmid pMD2.G	A gift from Didier Trono	RRID: Addgene_12259
Plasmid pHIT123	(Soneoka et al., 1995)	N/A
Plasmid psPAX2	A gift from Didier Trono	RRID: Addgene_12260
Software and algorithms		
MAGeCK	(Li et al., 2014)	N/A
STRING analysis	(Szklarczyk et al., 2019)	RRID: SCR_005223
Cutadapt (version 1.9.1)	(Martin, 2011)	RRID: SCR_011841
RSEM package (version 1.3.0)	(Li and Dewey, 2011)	RRID: SCR_013027
STAR alignment algorithm (version 2.5.2a)	(Dobin et al., 2013)	RRID: SCR_004463
Ensembl genome browser (assembly GRCm38, release 89)	(Kersey et al., 2016)	RRID: SCR_013367
DESeq2 package (version 1.12.3)	(Love et al., 2014)l	RRID: SCR_015687
R (version 3.3.1)	(R Core team, 2015)	N/A
MATLAB		Mathworks RRID: SCR_001622
Fiji-ImageJ	(Schindelin et al., 2012)	RRID: SCR_002285

(*Continued on next page*)

Continued

REAGENT or RESOURCE	SOURCE	IDENTIFIER
Flowjo™ Software for Mac OS X (Version 10.7.1)		BD RRID: SCR_008520
Graphpad Prism (Version 8.4.3)		Graphpad Software LLC RRID: SCR_002798

RESOURCE AVAILABILITY

Lead contact

Further information and requests for resources and reagents should be directed and will be fulfilled by the lead contact Pavel Tolar (p.tolar@ucl.ac.uk).

Materials availability

Plasmids and plasmid libraries generated in this study have been deposited to Addgene, LentiGuide Cherry, Plasmid #170510, Mouse Cherry Brie Pooled Library, Pooled Library #170511.

Supply of 40LB cells are subject to an MTA agreement (Dr Daisuke Kitamura).

Data and code availability

RNAseq data have been deposited at GEO (GEO: GSE166853) and are publicly available as of the data of publication. Accession numbers are listed in the key resources table. Microscopy data reported in this paper will be shared by the lead contact upon request. This paper does not report original code. Any additional information require to reanalyze the data reported in this paper is available from the lead contact upon request.

EXPERIMENTAL MODEL AND SUBJECT DETAILS

Animal experimental models

Mice used in this study were rederived onto the C57BL/6 background at the Francis Crick Institute. Cas9-GFP mice used were Gt(ROSA)26Sor$^{tm1.1(CAG-cas9*,-EGFP)Fezh}$ (MGI allele ID 5583838, RRID:IMSR_JAX:024858). For constitutive Cas9 expression the Cas9-GFP mice are crossed to a β-actin Cre driver (Lewandoski et al., 1997), for Cas9-GFP expression restricted to the B cell lineage, these mice were crossed with *Cd79a*$^{cre/+}$ mice. *Cd79a*$^{cre/+}$ mice used were C(Cg)-Cd79a$^{tm1(cre)Reth}$/EhobJ (MGI allele ID 101774, RRID:IMSR_JAX: 029412) (Hobeika et al., 2006). *Grb2*$^{fl/fl}$ mice used were B6.C(Cg)-*Grb2*$^{tm1.1Lnit}$/J (MGI allele ID 95805, RRID:IMSR_JAX: 020422). RAG1 KO mice used were (B6.129S7-*Rag1*^{tm1Mom}/J) MGI allele ID 1857241, RRID:IMSR_JAX: 002216 or Rag1^{tm1Bal} MGI allele ID 2448994 (Spanopoulou et al., 1994)). B6.SJL.CD45.1 mice used were (B6.SJL-*Ptprc*^{a} *Pepc*^{b} /BoyJ) MGI allele ID 2164701. Tissues were taken from mice aged between 8-15 weeks. All experiments were approved by the Francis Crick Institute Ethical Review Panel and the UK Home Office.

40LB cultures

Naïve primary mouse B cells were isolated as described below. 5x10^5 B cells were grown on 5x10^5 40LB feeder cells in each well of a 6 well plate. Cells were cultured at 37°C at 5% CO_2 in RPMI media (Sigma) supplemented with 10% heat-inactivated fetal bovine serum (FBS) (ThermoFisher), 100μM non-essential amino acids (ThermoFisher), 2mM L-Glutamine (ThermoFisher), 50μM 2-Mercaptoethanol (ThermoFisher) and Penicillin-Streptomycin (GE Healthcare Life Sciences). 100ng/ml IL-4 (Peprotech) was added into the culture media. Cells were cultured on the same feeders for 3 days before being moved onto new feeders and put into fresh media with IL-4 for a further 3 days. After 6 days culture in the presence of 40LB cells, the B cells were isolated from the feeders using the Feeder Removal Kit, mouse (Miltenyi Biotech) following manufacturer's instructions. B cells were then cultured for a further 2 days in RPMI (as described above) or supplemented with 500ng/ml anti-Igκ F(ab')$_2$ (Southern Biotech). Where indicated the following reagents were added into *in vitro* cultures: 100nM Rapamycin, 10nM Thapsigargin, 10μM Ru360 (all Sigma-Aldrich), 1μM BAY 61-3606 (Calbiochem).

METHOD DETAILS

Flow cytometry

Single cell suspensions were blocked with anti-CD16/32 for 20 minutes and incubated with Fixable Viability Dye-ef780 (ThermoFisher) for 20 minutes. Cells were subsequently stained with appropriate antibodies for 20 minutes on ice. The following stains and antibodies (for further details see key resources table) were used for immunophenotyping: B220 (RA3-6B2), CD138 (281-2), CD21/35 (eBio4E3), CD23 (B3B4), CD38 (90), CD4 (RM4-5), CD93 (AA4.1), CD95 (Jo2), IgD (11-26c), IgG1 (RMG1-1 or X56), IgM (R6-60.2), IgE (RME-1), TCRβ (H57-597). Cells were analyzed using an LSR-Fortessa flow cytometer. To measure

apoptosis, cells were stained using the Annexin V apoptosis detection kit (ThermoFisher) following manufacturer's instructions. Intracellular staining using antibodies detecting Active Caspase-3 (C92-605) and BCL2L11 (Y36) was performed using BD Cytofix/Cytoperm (BD Biosciences) or eBioscience FoxP3/Transcription Factor Staining Buffer Set (ThermoFisher). Intracellular staining using antibodies to detect IRF4 (3E4) and PRDM1 (5E7) was performed using True-Nuclear Transcription Factor Buffer Set (Biolegend). For mitochondrial stains, cells were loaded for 30 minutes at 37°C in the dark in HBSS with 500nM Mitotracker™ Green FM (ThermoFisher), 500nM MitoTracker™ Orange CMTM Ros (ThermoFisher), 100nM TMRM (AAT Bioquest) or 5μM Rhod-2 AM (ThermoFisher). Rhod-2 AM was loaded in the presence of 0.02% Pluronic F127 (ThermoFisher). Intracellular staining for phospho-S6 and phospho-mTOR (both from Cell Signaling Technology) using eBioscience FoxP3/Transcription Factor Staining Buffer Set (ThermoFisher). To analyse proliferation, cells were loaded for 20 minutes at 37°C in the dark in PBS with 5μM CellTrace™ Violet (ThermoFisher). Free dye was removed by incubating with five times volume of complete media for 5 minutes at 37°C.

Calcium flux analysis

IgG1$^+$ and IgE$^+$ B cells from the *in vitro* culture (8x10^6 cells) were loaded for 30 minutes at 37°C in the dark with 4.5μM Indo-1, AM (ThermoFisher) in the presence of 0.02% Pluronic F127 (ThermoFisher). Cells were then stained with surface antibodies or Fab fragments against IgE (made in-house) and IgG (Jackson ImmunoResearch Europe Ltd) at RT and resuspended in HBSS. Cells were pre-warmed to 37°C before analysis. After 60s of acquisition, cells were stimulated with 1μM Thapsigargin (Sigma-Aldrich). Samples were acquired for 8 minutes, before addition of 5μg/ml Ionomycin (Sigma-Aldrich). Indo-1 fluorescence emission was measured using which a 355nm laser and 450/50 (Indo-1 violet) and 530/50 (Indo-1 blue) filter sets on a BD LSR-Fortessa flow cytometer. The ratio was calculated as Indo-1 violet/Indo-1 blue. For microscopy, IgE$^+$ and IgG1$^+$ cells from *in vitro* cultures (1x10^6 cells) cultured with or without anti-Igκ F(ab')$_2$ were loaded with 1μM Fura Red™, AM (ThermoFisher) and 1μM Fluo-4, AM (ThermoFisher) in the presence of 0.02% Pluronic F127 (ThermoFisher). Cells were then stained with CD138 and labelled Fab fragments against IgE (made in-house) and IgG (Jackson ImmunoResearch Europe Ltd), and settled into poly-L-lysine coated Lab-Tek chambers (Nunc) in HBSS for imaging. The cells were imaged live over 10-20 min using an inverted Nikon Eclipse Ti microscope equipped with a 40x objective and a 37°C environmental control chamber. The samples were illuminated using 405, 488, 552 and 637 nm lasers (Cairn) controlled by iLas^2 laser illuminator (Gataca Systems). Images were captured on an ORCA-Flash 4.0 V3 digital complementary metal-oxide semiconductor (CMOS) camera (Hamamatsu Photonics) with a 3-second time resolution. The images were background subtracted and cells belonging to the indicated cell populations were identified by their fluorescence in the IgG, IgE and CD138 channels. The ratio of Fluoro4 to FuraRed fluorescence indicating calcium level was measured over time in each cell using ImageJ. Oscillations in the calcium traces were quantified using the findpeaks function in Matlab (Mathworks).

B cell purification and sorting

Naïve primary B cells were isolated from C57BL/6 or constitutive Cas9-GFP (described above) mice.

B cells from the spleen were isolated by negative selection using ACK lysis (made in house) and CD43 microbeads (Miltenyi Biotech), following manufacturer's instructions. To purify cultured B cells from 40LB feeders, the Feeder Removal Kit, mouse (Miltenyi Biotech) was used, following manufacturer's instructions. To purify IgE$^+$ and IgG1$^+$ cells for RNAseq or for CRISPR-Cas9 screens, cells were sorted according to the staining strategy as described below using a BD FACS Aria III or a BD FACS Aria Fusion. Sorted IgE$^+$ PC for culture with BAY 61-3606 were magnetically pre-enriched using negative selection and were stained using a Fab fragment against IgE (made in house) and anti-CD138.

RNAseq

B cells were isolated from the spleens of 3 C57BL/6 female mice (aged 11 weeks) using CD43 Microbeads (Miltenyi Biotech) as described previously. For each biological replicate, B cells were cultured on 2 6-well plates of 40LB feeders as described previously, in the presence of 100ng/ml IL-4 (Peprotech). B cells were removed from feeders as described previously and cultured in RPMI without stimulation for 2 days prior to sorting. Cells were sorted as follows: IgE iGC (IgE$^+$, CD138$^-$), IgG1 iGC (IgG1$^+$, CD138$^-$), IgE PC (IgE$^+$, B220^{lo}, CD138$^-$), IgG1 PC (IgG1$^+$, B220^{lo}, CD138$^-$). Sorted cells were immediately lysed in buffer RLT and samples were homogenized by pipetting back and forth through a 25G needle and frozen on dry ice. Samples were stored at -80°C until processed. Bulk d6 samples were taken from a separate B cell culture, as described above, using B cells isolated from the spleens of 3 C57BL/6 female mice (aged 8 weeks). B cells were removed from feeders using Feeder Removal Microbeads, mouse (Miltenyi Biotech) and cells were lysed and frozen as described above.

RNA was isolated from cells as using the RNeasy micro kit (Qiagen) for PC samples or the RNeasy mini kit (Qiagen) for iGC and bulk d6 samples as per manufacturer's instructions. RNA QC was performed by the Crick HTS (high-throughput sequencing) core facility using a Bioanalyzer (Agilent), all samples had a RIN score of 10. Stranded mRNA libraries were prepared in the Crick HTS facility using a KAPA mRNA HyperPrep Kit (Roche) and sequenced on the Illumina HiSeq 4000 platform (76bp single-end sequencing).

Bioinformatics for RNAseq

RNA sequencing was carried out on the Illumina HiSeq 4000 platform and typically generated ~44 million 76bp, strand-specific, single-end reads per sample. Adapter trimming was performed with cutadapt (version 1.9.1) (Martin, 2011) with parameters "–minimum-length=25 –quality-cutoff=20 -a AGATCGGAAGAGC". The RSEM package (version 1.3.0) (Li and Dewey, 2011) in conjunction with the STAR alignment algorithm (version 2.5.2a) (Dobin et al., 2013) was used for the mapping and subsequent gene-level counting of

the sequenced reads with respect to all *M. musculus* genes downloaded from the Ensembl genome browser (assembly GRCm38, release 89) (Kersey et al., 2016). The parameters used were ''–star-output-genome-bam –star-gzipped-read-file –forward-prob 0'', and all other parameters were kept as default.

Differential expression analysis was performed with the DESeq2 package (version 1.12.3) (Love et al., 2014) within the R programming environment (version 3.3.1) (R Development Core Team, 2015). An adjusted p-value of $\leq$ 0.01 was used as the significance threshold for the identification of differentially expressed genes.

The RNAseq data are available in the Gene Expression Omnibus (GEO) database (http://www.ncbi.nlm.nih.gov/gds) under the accession number GSE166853 (GEO: GSE166853).

Production of mouse sgRNA Cherry Brie Library

LentiGuide-Cherry plasmid was produced by restriction digest cloning, replacing the Puromycin selection cassette in LentiGuide-Puro (Addgene #52963) with the sequence encoding mCherry. The Cherry Brie pooled CRISPR library was obtained by Gibson assembly cloning to place the sgRNA sequences form the Mouse Brie CRISPR knockout pooled library (a gift from David Root and John Doench (Addgene #73633)) into the LentiGuide-Cherry plasmid (Figure S1A). The cloned library was expanded in Electrocompetent E.coli (Lucigen) and sequence complexity was analyzed using next generation sequencing using an Illumina MiSeq. Pooled lentiviral libraries were subsequently produced as described below.

Lentivirus production

Replication incompetent lentiviruses were produced by co-transfecting $5x10^6$ HEK293T cells with 10μg vector plasmid LentiGuide-Cherry or Cherry Brie, 5μg envelope plasmid pMD2.G (A gift from Didier Trono (Addgene #12259)) or pHIT123 (Soneoka et al., 1995) and 7.5μg packaging plasmid psPAX2 (A gift from Didier Trono (Addgene #12260)) in opti-MEM media (ThermoFisher) using transit-LT1 transfection reagent (Mirus bio LLC). Lentivirus was harvested 48 and 72 hours post-transfection and concentrated by ultracentrifugation. Lentivirus production was scaled up where necessary for production of lentiviral library. Genomic DNA was isolated from HEK293T cells using DNeasy Blood and Tissue Kit (Qiagen) following manufacturer's instructions.

CRISPR screens and analysis

Naïve primary mouse B cells were isolated from constitutive Cas9-GFP spleens as described above. $50x10^6$ primary B cells were spin-infected for 90mins at 2300rpm in the presence of 16μg/ml polybrene (Millipore) with pooled whole-genome Cherry-Brie lentiviral CRISPR libraries at an MOI of 0.3 to obtain 200-fold coverage of the library. Transduced B cells were cultured on 40LB feeder cells as described previously, Bcells were removed from feeders and cultured in RPMI without stimulation or with anti-Igκ $F(ab')_2$ as a surrogate antigen for 2 days prior to sorting. To isolate IgE^+ B cells from CRISPR-Cas9 screen cultures, IgE^+ cells were first enriched by negative selection, removing IgM^+ and $IgG1^+$ cells using biotinylated antibodies and streptavidin conjugated microbeads (Miltenyi Biotech). To isolate $IgG1^+$ B cells from CRISPR-Cas9 screen cultures, $IgG1^+$ cells were first enriched by negative selection, removing IgM^+ and IgE^+ cells using biotinylated antibodies and streptavidin conjugated microbeads (Miltenyi Biotech). Successfully transduced, $mCherry^+$ cells were sorted as described for RNAseq experiments. Where necessary cells were pooled from multiple sorts to ensure library coverage, with a minimum of $3x10^6$ sorted cells used per library. Genomic DNA was isolated from sorted cells using the DNeasy Blood and Tissue Kit (Qiagen) following manufacturer's instructions. The integrated viral genome was amplified using a nested PCR (primers as described in key resources table). Libraries were sequenced using an Illumina MiSeq or HiSeq (100bp paired-end sequencing). Raw reads in demultiplexed FASTQ files were trimmed to identify sgRNA sequences and aligned to the Brie library sequences using Bowtie. The frequency of aligned read counts for each sgRNA was calculated using MATLAB (Mathworks). CRISPR scores calculation and statistical analysis was performed using MAGeCK (Li et al., 2014).

$$\text{CRISPR score} = \log2\left(\frac{1+\text{sgRNA abundance sorted population}}{1+\text{sgRNA abundance relevent HEK293T library}}\right)$$

To compare CRISPR scores for the different populations, which were analyzed in separate experiments, CRISPR scores in each population were normalized using:

$$\text{CRISPR score norm} = \frac{\text{CRISPR score} - \text{meanCSnonTargetingExp}}{\frac{\text{meanCSEssentialExp}}{\text{meanCSEssentialAllExp}}}$$

Where meanCSnonTargetingExp is the mean CRISPR score of the non-targeting guides in this experiment, meanCSEssentialExp is the mean CRISPR score of the 187 essential genes (Figure S1) in this experiment and meanCSEssentialAllExp is the mean CRISPR score of the 187 essential genes in all experiments.

For population specific gene lists (Tables S3–S6), normalized CRISPR score data was filtered using cut-offs as described in relevant supplemental Tables.

CRISPR-mediated gene disruption

CRISPR sgRNA sequences were designed using the Broad Institute sgRNA Designer. Forward and reverse oligonucleotide sequences including the guide sequence were synthesized, phosphorylated, annealed and individually cloned into lentiGuide-Cherry.

Lentivirus was produced and B cells or HSCs were spin-infected as described above. For gene targeting in HSCs, the pMD2.G envelope was used, and for primary B cells, the pHIT123 envelope was used. HSCs were isolated using CD117 beads (Miltenyi Biotech) following manufacturer's instructions. Spin-infected HSCs were cultured overnight in StemSpan media (StemCell Technologies) in the presence of 100ng/ml mSCF, 6ng/ml IL-3, 10ng/ml hIL-6, 20ng/ml TPO, 60ng/ml Flt3L (all Peprotech).

Amplicon sequencing for detection of indels

Genomic DNA was isolated from non-targeted primary B cells or from transduced B cells at day 8 of in vitro cultures using the DNeasy Blood and Tissue Kit (Qiagen) following manufacturer's instructions. PCR was performed to amplify a region of interest surrounding the sgRNA binding site with overhand adapters (primers as described in key resources table). Indexed Illumina sequencing adapters were then added during a limited-cycle amplification step. DNA libraries were normalised and pooled after fluorometric quantification using a dsDNA dye. Pooled libraries were sequenced using an Illumina MiSeq (250bp paired-end sequencing). Frequency of Indels was calculated using CRISPR RGEN Tools Cas-Analyzer (Park et al., 2017). Transduction efficiency was assessed as proportion of mCherry^{+} cells, analysed by flow cytometry, at day 8 of *in vitro* cultures.

Lentiviral chimeras

For bone marrow chimeras B6.SJL.CD45.1 (B6.SJL-*Ptprc*^{a} *Pepc*^{b} /BoyJ) recipient mice were lethally irradiated (10Gy split dose) or RAG-1 KO recipient mice ((B6.129S7-*Rag1*^{tm1Mom}/*J*) or Rag1^{tm1Bal} (Spanopoulou et al., 1994))) were sub-lethally irradiated (5Gy) and reconstituted with 1-1.5x10^{6} lentivirally transduced (described above) cKit^{+} donor constitutive Cas9-GFP or *Cd79*$^{Cre/+}$ LSL-Cas9-GFP hematopoietic stem cells (HSCs) by intra-venous injection. Reconstituted mice were fed 0.2mg/ml Baytril (Enrofloxacin) in their drinking water for 4 weeks post-reconstitution. Mice were bled to ensure successful reconstitution and were immunized at 8-11 weeks. Mice were immunized sub-cutaneously with 50μl NP-CGG (2B Scientific) (1mg/ml in PBS) mixed 1:1 with Imject Alum Adjuvant (ThermoFisher) in the upper and lower flank to target the brachial, axillary and inguinal draining LNs. Mouse tissues were analyzed by flow cytometry 1 week post-immunization.

qPCR

RNA was isolated from sorted cells using RNeasy micro kit (Qiagen) or RNeasy mini kit (Qiagen), depending on cell number, following manufacturer's instructions. cDNA was prepared using the QuantiTect Reverse Transcription Kit (Qiagen). qPCR to assess transcript abundance of Irf4, Tbp and Hprt was performed using the following assays: Mm00516431_m1 (Irf4), Mm01277042_m1 (Tbp), and Mm03024075_m1 (Hprt) (Applied Biosystems) using TaqMan Fast Advanced Master Mix (Applied Biosystems) following manufacturer's instructions. qPCRs were performed using a ViiA 7 Real-Time PCR System (Applied Biosystems).

Microscopy of mitochondria

Epifluorescence and TIRF imaging were carried out on a Nikon Eclipse Ti microscope with an ORCA-Flash 4.0 V3 digital complementary metal-oxide semiconductor (CMOS) camera (Hamamatsu Photonics) and 100x TIRF objective (Nikon). Illumination was supplied by 405, 488, 552 and 637 nm lasers (Cairn) through an iLas^{2} Targeted Laser Illuminator (Gataca Systems) which produces a 360° spinning beam with adjustable TIRF illumination angle.

Primary B cells from the *in vitro* cultures were stained as described previously before being added to 0.05% Poly-L lysine coated 8-well Lab-Tek imaging chambers (ThermoScientific) and allowed to interact at 37°C. Cells were imaged live. Acquired datasets were analyzed using MATLAB with ImageJ plugin as previously described (Nowosad et al., 2016). Briefly, individual cells were segmented using brightfield and cell surface staining and their fluorescence in the channels showing membrane IgE, IgG1, B220 and CD138 was plotted to allow gating on the desired populations as described for flow cytometry. Mitochondria in gated cells were analyzed by segmenting individual MitoTracker^{TM} Green spots and recording their number and fluorescence.

QUANTIFICATION AND STATISTICAL ANALYSIS

Graphs were made and statistics performed using Graphpad Prism. Details of statistical tests and sample sizes are indicated in figure legends, p values are indicated in the figures.